Novel calmodulin variant p.E46K associated with severe CPVT produces robust arrhythmogenicity in human iPSC-derived cardiomyocytes

Short title: Modeling CaM-related CPVT using iPS cells

Jingshan Gao, MSc[1], Takeru Makiyama, MD, PhD[1,2]*, Yuta Yamamoto, DVM, PhD[1,3], Takuya Kobayashi, PhD[4], Hisaaki Aoki, MD, PhD[5], Thomas L. Maurissen, PhD[6], Yimin Wuriyanghai, MD, PhD[1], Asami Kashiwa, MD, PhD[1], Tomohiko Imamura, MD[1], Takanori Aizawa, MD[1], Hai Huang, MSc[1], Hirohiko Kohjitani, MD, PhD[1], Misato Nishikawa[7], Kazuhisa Chonabayashi, MD, PhD[7,8], Megumi Fukuyama, MD, PhD[9], Hiromi Manabe, MD[10], Kouichi Nakau, MD[11], Tsutomu Wada, MD, PhD[12], Koichi Kato, MD, PhD[9], Futoshi Toyoda, PhD[13], Yoshinori Yoshida, MD, PhD[7], Naomasa Makita, MD, PhD[14], Knut Woltjen, PhD[6], Seiko Ohno, MD, PhD[3], Nagomi Kurebayashi, PhD[4], Takashi Murayama, PhD[4]*, Takashi Sakurai, MD, PhD[4], Minoru Horie, MD, PhD[9], Takeshi Kimura, MD, PhD[1]

[1] Department of Cardiovascular Medicine, Kyoto University Graduate School of Medicine, Kyoto, Japan

[2] Department of Community Medicine Supporting System, Kyoto University Graduate School of Medicine, Kyoto, Japan

[3] Department of Bioscience and Genetics, National Cerebral and Cardiovascular Center, Suita, Japan

[4] Department of Pharmacology, Juntendo University School of Medicine, Tokyo, Japan

[5] Department of Pediatric Cardiology, Osaka Women's and Children's Hospital, Osaka, Japan

[6] Department of Life Science Frontiers, Center for iPS Cell Research and Application (CiRA), Kyoto University, Kyoto, Japan

[7] Department of Cell Growth and Differentiation, Center for iPS Cell Research and Application (CiRA), Kyoto University, Kyoto, Japan

[8] Department of Hematology and Oncology, Kyoto University Graduate School of Medicine, Kyoto, Japan

[9] Department of Cardiovascular Medicine, Shiga University of Medical Science, Otsu, Japan

[10] Department of Pediatrics, Asahikawa Kosei General Hospital, Asahikawa, Japan

[11] Department of Pediatrics, Asahikawa Medical University, Asahikawa, Japan

[12] Department of Pediatrics, Sapporo Medical University Hospital, Sapporo, Japan

[13] Department of Physiology, Shiga University of Medical Science, Otsu, Japan

[14] Omics Research Center, National Cerebral and Cardiovascular Center, Suita, Japan

Y. Yamamoto's present address: Division of Cardiovascular Medicine, Department of Medicine, Stanford University, Stanford, CA, United States.

T. L. Maurissen's present address: Roche Pharma Research and Early Development, Immunology, Infectious Diseases and Ophthalmology, Roche Innovation Center Basel, F. Hoffmann-La Roche Ltd., Basel, Switzerland.

Y. Wuriyanghai's present address: Department of Internal medicine, Peking University Third Hospital, Beijing, China.

N. Makita's present address: Department of Cardiology, Sapporo Teishinkai Hospital, Sapporo, Japan.

T. Kimura's present address: Department of Cardiology, Hirakata Kohsai Hospital, Osaka, Japan.

***Co-correspondence to:**

Takeru Makiyama, MD, PhD

Department of Community Medicine Supporting System, Department of Cardiovascular Medicine, Kyoto University Graduate School of Medicine,

54 Shogoin Kawahara-cho, Sakyo-ku, Kyoto, 606-8507, Japan.

Tel: +81-75-751-4255, Fax: +81-75-751-3299.

E-mail: makiyama@kuhp.kyoto-u.ac.jp

Takashi Murayama, PhD

Department of Pharmacology, Juntendo University School of Medicine.

2-1-1 Hongo, Bunkyo-ku, Tokyo 113-8421, Japan.

Tel: +81-3-5802-1035, Fax: +81-3-5802-0419.

E-mail: takashim@juntendo.ac.jp

Total word count of the manuscript: 9272 words

Abstract

Background:

Calmodulin (CaM) is a ubiquitously expressed, multifunctional Ca^{2+} sensor protein that regulates numerous proteins. Recently, CaM missense variants have been identified in patients with malignant inherited arrhythmias, such as long QT syndrome (LQTS) and catecholaminergic polymorphic ventricular tachycardia (CPVT). However, the exact mechanism of CaM-related CPVT in human cardiomyocytes (CMs) remains unclear. In this study, we sought to investigate the arrhythmogenic mechanism of CPVT caused by a novel variant using human induced pluripotent stem cell (iPSC) models and biochemical assays.

Methods:

We generated iPSCs from a CPVT patient bearing *CALM2* p.E46K. As comparisons, we utilized two control lines including an isogenic line, and another iPSC line from an LQTS patient bearing *CALM2* p.N98S (also reported in CPVT). Electrophysiological properties were investigated using iPSC-CMs. We further examined the cardiac ryanodine receptor (RyR2) and Ca^{2+} affinities of CaM using recombinant proteins.

Results:

We identified a novel *de novo* heterozygous variant, *CALM2* p.E46K, in two unrelated CPVT patients accompanied by neurodevelopmental disorders. The E46K-CMs exhibited more frequent abnormal electrical excitations and Ca^{2+} waves than the other lines in association with increased Ca^{2+} leakage from the sarcoplasmic reticulum via RyR2. Furthermore, the [^{3}H]ryanodine binding assay revealed that E46K-CaM facilitated RyR2 function especially by activating at low [Ca^{2+}] levels. The real-time

CaM-RyR2 binding analysis demonstrated that E46K-CaM had a tenfold increased RyR2 binding affinity compared to wild-type CaM which may account for the dominant effect of the mutant CaM. Additionally, the E46K-CaM did not affect CaM-Ca^{2+} binding or L-type calcium channel function. Finally, antiarrhythmic agents, nadolol and flecainide, suppressed abnormal Ca^{2+} waves in E46K-CMs.

Conclusions:

We, for the first time, established a CaM-related CPVT iPSC-CM model which recapitulated severe arrhythmogenic features resulting from E46K-CaM dominantly binding and facilitating RyR2. In addition, the findings in iPSC-based drug testing will contribute to precision medicine.

Key words: calmodulin, catecholaminergic polymorphic ventricular tachycardia, induced pluripotent stem cell, cardiac ryanodine receptor, sudden death

Non-standard Abbreviations and Acronyms

CaM	**calmodulin**
LTCC	**L-type calcium channel**
RyR2	**cardiac ryanodine receptor**
LQTS	**long QT syndrome**
CPVT	**catecholaminergic polymorphic ventricular tachycardia**
AP	**action potential**
CDI	**Ca^{2+}-dependent inactivation**
SR	**sarcoplasmic reticulum**
iPSC-CM	**induced pluripotent stem cell-derived cardiomyocyte**
WT	**wild-type**
EB	**embryoid body**
I_{CaL}	**L-type calcium channel current**
ER	**endoplasmic reticulum**
$[Ca^{2+}]_{cyt}$	**cytoplasmic Ca^{2+} concentration**
$[Ca^{2+}]_{ER}$	**endoplasmic reticulum luminal Ca^{2+} concentration**
BLI	**biolayer interferometry**
ACMG	**American College of Medical Genetics and Genomics**
PDA	**patent ductus arteriosus**
HR	**heart rate**
PVC	**premature ventricular contraction**
E46K-Cor	***CALM2* p.E46K gene-corrected isogenic control**
SNP	**single nucleotide polymorphism**
MLC2a	**atrial myosin light chain 2**

132	**MLC2v**	**ventricular myosin light chain 2**
133	**EAD/DAD**	**early/delayed afterdepolarization**
134	**APD_{50}/APD_{90}**	**action potential duration at 50%/90% repolarization**
135	**CV**	**conduction velocity**
136	**k_{on}**	**association rate**
137	**k_{off}**	**dissociation rate**
138	**K_D**	**binding affinity constant**
139	**cryo-EM**	**cryogenic electron microscopy**

140

Introduction

Calmodulin (CaM) is an essential intermediate calcium-binding messenger protein and regulates numerous cellular systems in response to Ca^{2+} signals.[1] In the heart, CaM also has many target proteins,[2] and among them, L-type calcium channels (LTCC) and cardiac ryanodine receptors (RyR2) are considered to play important roles in relation to arrhythmias.[3, 4]

To date, approximately 30 CaM variants have been identified in patients with life-threatening arrhythmic syndromes, such as long QT syndrome (LQTS)[5, 6] and catecholaminergic polymorphic ventricular tachycardia (CPVT)[7]. Previous studies elucidated that the CaM variants found in LQTS prolonged action potential (AP) durations in association with delayed Ca^{2+}-dependent inactivation (CDI) of the LTCCs by decreasing CaM affinity to Ca^{2+}.[8, 9] It has been also theorized that the CaM variants associated with CPVT can increase the open probability of RyR2 channels and enhance the Ca^{2+} leakage from the sarcoplasmic reticulum (SR), which is an underlying mechanism of CPVT.[10, 11]

In humans, CaM is encoded by three different genes (*CALM1*, *CALM2*, and *CALM3*) which produce identical amino acid sequences.[12] In hearts, all three *CALM* genes are expressed.[5] Most CaM variants have a dominant effect, suggesting that the variant in only one out of six CaM alleles is enough to cause arrhythmias.[5-7, 11] However, it remains unclear how such strong effect is caused by only one mutated allele.

The present study, for the first time, investigated a CaM-related CPVT variant using patient-specific induced pluripotent stem cell-derived cardiomyocyte (iPSC-CM) models, which reproduce patients' cardiomyocytes including an expression ratio of

wild-type (WT) and mutated CaMs[8]. The iPSC-CMs bearing a novel variant, *CALM2* p.E46K showed enhanced afterdepolarizations and abnormal Ca^{2+} waves associated with severe SR Ca^{2+} leak. Further biochemical assays revealed that E46K-CaM facilitated RyR2 with dramatically increased binding affinity compared to WT-CaM. In addition, antiarrhythmic agents, nadolol and flecainide, suppressed the abnormal Ca^{2+} waves in E46K iPSC-CMs, which provides a contribution in developing precision medicine.

Methods

The data that support the findings of this study are available from the corresponding author upon reasonable request. Detailed descriptions of materials and methods are available in the Supplemental methods.

Study approval

Derivation and use of human iPSCs were approved by the Kyoto University ethics review board (G259) and conformed to the principles of the Declaration of Helsinki. All subjects provided informed consents prior to the participation.

Clinical data and target exome sequencing

Clinical data and genetic analyses were performed through targeted gene sequencing of 60 genes (Table S1).[13]

Generation of iPSCs, establishment of the isogenic control, and cardiac differentiation

Patient-specific iPSC clones were generated from a patient carrying the *CALM2* p.E46K

by reprogramming of peripheral blood mononuclear cells. Further, iPSC lines generated from a healthy individual and an isogenic iPSC line corrected using CRISPR/Cas9-mediated gene editing[14] were used as controls. The iPSCs were differentiated into CMs using an embryoid body (EB) differentiation system as previously described.[15, 16] The primers used for sequencing of on-target and off-target sites and quantitative PCR are listed in Table S2. More than two independent clones of each cell line were used in each experiment. All experimental data were collected from at least 3 independent differentiations.

Immunocytochemistry

The expression of pluripotency markers in iPSCs and the expression of sarcomere-related proteins in iPSC-CMs were analyzed by immunostaining.

Electrophysiological analysis in iPSC-CMs

We utilized optical techniques in AP recordings, Ca^{2+} transient recordings, and Ca^{2+} homeostasis analysis. In addition, we recorded APs and LTCC currents (I_{CaL}) using a whole-cell patch-clamp technique.[17, 18]

Imaging of Ca^{2+} dynamic in the cytosol and endoplasmic reticulum (ER) in HEK293 cells expressing RyR2 channels

Cytoplasmic Ca^{2+} ($[Ca^{2+}]_{cyt}$) signals in the HEK293 cells expressing WT RyR2 channels and WT/mutant CaMs were measured with Fluo-4.[19, 20] The ER luminal Ca^{2+} ($[Ca^{2+}]_{ER}$) signals were measured with genetically encoded Ca^{2+} sensor proteins, R-CEPIA1er, in separate measurements.[20]

[^{3}H]Ryanodine binding assay

[^{3}H]Ryanodine binding was performed on HEK293 cell microsomes.[21]

Biolayer interferometry (BLI)-based CaM-RyR2 binding assay

The BLI analyses were performed with the Octet RED 96 system (ForteBio, Fremont, CA, USA). The data were processed and analyzed using the Octet Data Analysis Software 9.0 (ForteBio).

Measurement of Ca^{2+}-CaM binding affinity

Ca^{2+}-binding affinity of CaMs (WT, E46K, and N98S) were determined by monitoring the intrinsic tyrosine and phenylalanine fluorescence during a Ca^{2+} titration as previously described.[22]

Statistical analysis

Statistical comparisons were performed using Student's *t*-test for paired observations. One-way analysis of variance (ANOVA) was performed when multiple independent groups were compared. Post hoc comparisons between individual means were performed by Tukey's method and *p*-values have been corrected for multiple testing. A *p*-value of <0.05 was considered statistically significant.

Results

Identification of a *de novo* heterozygous variant in *CALM2* gene, p.E46K in two unrelated CPVT patients

In two unrelated Japanese CPVT patients with neurodevelopmental disorders, we conducted a targeted next generation sequencing of 60 genes related to arrhythmias

(Table S1) and identified a heterozygous variant, c.136G>A, p.E46K in *CALM2*. The variant was not reported in any genomic variation databases nor in normal populations. Genetic testing of their family members revealed that it was a *de novo* variant (Figure 1A and B). The variant, p.E46K, is located in the linker of two EF-hand motifs which are in the CaM N-domain, where the position is close to the previously reported CPVT-related variant, p.N54I (Figure 1C).[7] In the genetic analysis, we identified 4 other rare variants except for *CALM2* p.E46K (Table S3). According to the American College of Medical Genetics and Genomics (ACMG) classification[23], three of them are classified as benign, and a rare variant, *TRPM4* p.I1033N, in proband 2 is classified as a variant of uncertain significance. Since *TRPM4* p.I1033N was also found in his asymptomatic father, the variant is unlikely to be responsible for the CPVT phenotype.

Clinical characterization of two CPVT probands

Proband 1 is currently a 15-year-old male. He had patent ductus arteriosus (PDA) at birth and presented signs of an intellectual disability at the age of 1. At 10 years old, he had several syncopal episodes while running. His resting ECG showed sinus bradycardia with a heart rate (HR) of 50 bpm and prominent U waves in V_1 and V_2 leads (Figure 1D). His HR during sleep was 35 bpm (data not shown). His Holter ECG and exercise test showed adrenergic-induced polymorphic ventricular tachycardias (VTs) (Figure 1D and Figure S1). After being clinically diagnosed with CPVT, he was started on nadolol (30-40 mg/day) which has been effective in preventing syncopal attacks and VTs. Since frequent premature ventricular contractions (PVCs) were observed at the age of 15, flecainide acetate was additionally prescribed.

Proband 2 is currently a 17-year-old male. At the gestational age of 28 weeks and 1

day, an emergent cesarian section was performed due to severe fetal bradycardia with a HR range of 80-90 bpm. His birth weight was 1098 g. Subsequently, he underwent a bowel resection due to necrotizing enterocolitis and a PDA surgery. At the age of 5, he was diagnosed with an intellectual disability and autism spectrum disorder. His resting ECG showed bradycardia with a HR of 55 bpm, and bidirectional VTs were recorded by Holter ECG during exercise (Figure 1E). After a diagnosis of CPVT, β-blockers were prescribed. Due to poor compliance associated with his neurodevelopmental disorders, he had one syncopal episode under emotional stress at the age of 14 and an aborted cardiac arrest at 16 years old. The patient has been treated with carvedilol (5 mg/day) and flecainide acetate (100 mg/day), and no further cardiac events have occurred following strict compliance.

The unequivocal CPVT features together with other clinical phenotypes, such as sinus bradycardia, a similar T-U wave morphology, PDA, and neurodevelopmental disorders detected in both probands suggested a strong pathogenicity of this novel variant, *CALM2* p.E46K.

Generation of the patient-derived iPSC and gene-corrected isogenic control iPSC lines

To investigate the impacts of this novel CaM-related CPVT variant in human CMs, a patient-derived iPSC line bearing *CALM2* p.E46K was generated from the first proband (Family 1, Figure 1A). A control (Ctr) cell line, 201B7 iPSCs established from a healthy individual was utilized.[15, 24] To eliminate the effects of variable gene backgrounds, a gene-corrected isogenic control (E46K-Cor) iPSC line was generated from E46K iPSCs using CRISPR/Cas9-based gene editing methods (Figure S2A).[14] The genetic integrity

of E46K-Cor iPSCs was confirmed by Sanger sequencing. A heterozygous single nucleotide polymorphism (SNP) at 856 bases downstream of the variant was identified in both E46K and E46K-Cor iPSCs, which indicates that there are no unintended on-target mutations such as large deletions or insertions induced by the CRISPR-Cas9 (Figure S2B). As for the off-target genetic alterations, we did not detect any unexpected mutations in the three most potential off-target positions (Table S4). Furthermore, to compare the functional effects of E46K with other CaM variants, we utilized a previously established iPSC line from an LQTS patient bearing *CALM2* p.N98S,[8, 25] which was also reported in CPVT patients.[26]

Characterization of iPSCs and iPSC-CMs

Both E46K and E46K-Cor iPSC colonies exhibited morphological features of human embryonic stem cells, were positively stained with pluripotency markers (SSEA-4, TRA-1-60, and OCT3/4; Figure S3A), and maintained a normal karyotype (Figure S3B). All the iPSC lines were differentiated into CMs, and metabolic purification[27] and hormone-based maturation[28] were used (Figure S4A). The CMs differentiated from the iPSC lines (Ctr, E46K, and E46K-Cor) showed similar morphology and sarcomere organization stained with anti-cardiac troponin T antibody (Figure S4B). The percentage of CM subtypes was analyzed by staining for atrial and ventricular myosin light chain 2 (MLC2a and MLC2v) (Figure S4C). In Ctr, E46K, and E46K-Cor iPSC-CMs, more than 90% of CMs were positively stained with MLC2v, indicating a high proportion of ventricular-type iPSC-CMs (Figure S4D). In addition, the iPSC-CMs showed equivalent mRNA expression levels in the CPVT-related genes (*RYR2*, *ATP2A2*, *CASQ2*, and *CALM1-3*) and the genes associated with ion channels (*CACNA1C*,

298 *KCNQ1*, *SCN5A*, and *SLC8A1*) (Figure S4E).

299 **E46K iPSC-CMs exhibit frequent abnormal depolarizations in AP recordings**

300 To test the arrhythmogenicity of the novel CaM variant, we initially recorded APs in
301 iPSC-CM monolayers differentiated from various iPSC lines (Ctr, E46K, E46K-Cor,
302 and N98S) (Figure 2A and B) using a voltage-sensitive fluorescent dye. At baseline, Ctr,
303 E46K-Cor, and N98S cells exhibited regular APs evoked by 1 Hz electrical stimulations
304 with almost no abnormal depolarizations (Figure 2A and C). In contrast, E46K
305 occasionally showed abnormal depolarizations presented as both early and delayed
306 afterdepolarizations (EADs/DADs) and triggered activities (Figure 2A and C). Next, we
307 evaluated AP durations (APDs) at 50% and 90% repolarizations (APD_{50} and APD_{90})
308 and no significant differences were observed among the Ctr, E46K, and E46K-Cor. In
309 contrast, APDs were significantly prolonged in N98S compared to Ctr (Figure 2D and
310 Figure S5), which is consistent with our previous report[8].

311 Abnormal depolarizations were further increased in E46K in the presence of 100 nM
312 isoproterenol (Figure 2B and C). N98S showed few abnormal depolarizations even in
313 the presence of isoproterenol. Same as baseline condition, in the presence of
314 isoproterenol, APDs in E46K were similar as Ctr; in contrast, APDs in N98S were
315 significantly longer than the other cell lines (Figure 2D and Figure S5). The conduction
316 velocity (CV) was analyzed using AP maps of the iPSC-CM sheets under 1 Hz pacing.
317 There was no significant difference in CV among Ctr, E46K, and E46K-Cor at baseline
318 or in the presence of isoproterenol (Figure S6).

319 We next performed AP recordings using a whole-cell patch-clamp technique with
320 dissociated single iPSC-CMs, and we analyzed the AP waveforms and

electrophysiological parameters in detail.[29] DADs were occasionally identified in E46K during spontaneous beating (Figure S7A). Ctr, E46K, and E46K-Cor showed similar AP amplitude, maximum diastolic potential, APD_{90}, and APD_{50} during spontaneous beating and under 1 Hz pacing (Figure S7A and B, and Table S5).

CALM2 p.E46K promotes abnormal intracellular Ca^{2+} release

In CPVT, intracellular Ca^{2+} mishandling is thought to be an underlying mechanism of arrhythmias.[10] We therefore tested the effect of *CALM2* p.E46K on intracellular Ca^{2+} transient (Figure 3A and B). At baseline, regular Ca^{2+} transients were observed with few abnormal Ca^{2+} signals in Ctr and E46K-Cor. In contrast, E46K and N98S exhibited frequent abnormal Ca^{2+} release signals which occurred as abnormal Ca^{2+} waves, while the frequency in N98S is lower than E46K. In the presence of isoproterenol, E46K and N98S exhibited significantly more frequent abnormal Ca^{2+} waves than Ctr and E46K-Cor (Figure 3A and C). In addition, at baseline, the Ca^{2+} transient amplitude in E46K was significantly smaller compared to the other cell lines (Figure 3A and D). After the treatment with 100 nM isoproterenol, the Ca^{2+} transient amplitudes were significantly decreased in both E46K and N98S (Figure 3B and D), suggesting increased Ca^{2+} leak from SR in these cells.

We further compared the characteristics of abnormal Ca^{2+} waves in E46K and N98S (Figure S8A). E46K exhibited significantly higher amplitudes and earlier onset of abnormal Ca^{2+} waves compared to N98S (Figure S8B). Our data indicates that both variants, E46K and N98S, disturbed Ca^{2+} handling in iPSC-CMs and E46K is more arrhythmogenic than N98S.

E46K iPSC-CMs exhibit enhanced SR Ca^{2+} leak and reduced SR Ca^{2+} load

To dissect the underlying mechanisms of how two CaM variants altered Ca^{2+} handling, RyR2-mediated SR Ca^{2+} leakage (SR Ca^{2+} leak) and Ca^{2+} storage capacity of the SR (SR Ca^{2+} load) were assessed in single isolated iPSC-CMs (Figure 4A).[30] Compared to Ctr and E46K-Cor, the SR Ca^{2+} leak was significantly increased in the mutant CMs, E46K and N98S (Figure 4B), conversely, the SR Ca^{2+} load was dramatically reduced in the mutant CMs (Figure 4C). Specifically, E46K exhibited significantly larger alterations in the SR Ca^{2+} leak and SR Ca^{2+} load than N98S (Figure 4B and C). These data indicate that the severe SR dysfunction is accountable for the arrhythmogenicity in the CMs bearing disease variants and the larger SR Ca^{2+} leakage in E46K resulted in more severe arrhythmogenic features than N98S.

E46K-CaM markedly facilitates ER Ca^{2+} release in HEK293 cells expressing RyR2 channels

The above results suggest abnormal function of RyR2 in iPSC-CMs carrying *CALM* p.E46K variant. Since CaM interacts with many proteins including ion channels and transporters,[2] it is difficult to conclude whether the mutated CaM directly affects RyR2 function. We therefore tested the effect of mutated CaMs on HEK293 cells that stably express RyR2 without expressing other cardiac specific proteins.[19, 20] WT and mutated (E46K and N98S) CaMs were exogenously expressed using baculovirus vectors. The expression levels of CaMs were comparable among the three types of cell lines (WT, E46K, and N98S) (Figure S9).

We initially measured cytoplasmic Ca^{2+} using Fluo-4 in RyR2-HEK293 cells which exhibit spontaneous Ca^{2+} oscillations (Figure 5A).[19, 20] E46K exhibited more frequent Ca^{2+} oscillations compared to WT. Ca^{2+} oscillations were also enhanced in N98S;

however, the frequency was lower than in E46K (Figure 5A and B).

We next measured $[Ca^{2+}]_{ER}$ levels using R-CEPIA1er, a genetically-encoded ER Ca^{2+} indicator, because ER Ca^{2+} is a good measurement of RyR2 activity since higher RyR2 activity causes more ER Ca^{2+} leak, leading to lower $[Ca^{2+}]_{ER}$ levels.[20] During Ca^{2+} oscillations, the R-CEPIA1er signal reached a maximal level (threshold), rapidly decreased to a minimal level, and then gradually increased again toward the threshold (Figure 5C). The $[Ca^{2+}]_{ER}$ threshold levels were significantly reduced in E46K compared to WT (Figure 5D), indicating increased Ca^{2+} leakage from the ER. Slight but significant reduction of $[Ca^{2+}]_{ER}$ threshold levels were also observed in N98S. Taken together, these data suggest that E46K-CaM activates RyR2 to cause abnormal Ca^{2+} handling.

E46K-CaM facilitates RyR2 function, especially by activation at low Ca^{2+} levels

To investigate how E46K-CaM affects RyR2 channels, we employed a [^{3}H]ryanodine binding assay, which is useful in measuring the RyR2 channel activity.[31] Ca^{2+} dependence of [^{3}H]ryanodine binding showed the bell-shaped Ca^{2+} dependence curves with Ca^{2+} activation and inactivation phases.[19, 20] WT-CaM suppressed [^{3}H]ryanodine binding at all $[Ca^{2+}]$ levels (Figure 5E), indicating an inhibitory effect on RyR2 channels. In contrast, mutated CaMs (E46K and N98S) showed significantly higher [^{3}H]ryanodine binding levels than WT-CaM at specific $[Ca^{2+}]$ levels (E46K: pCa $\leq$ 5.43; N98S: pCa from 5.0 to 5.43), indicating that mutated CaMs failed to inhibit RyR2 channels (Figure 5F). Specifically, E46K-CaM showed significantly higher [^{3}H]ryanodine binding levels than N98S-CaM at pCa from 2.54 to 5.43 (Figure 5F).

To elucidate the precise physiological role of mutated CaMs in regulating the RyR2

activity, we analyzed the binding of [^{3}H]ryanodine to RyR2 at specific [Ca^{2+}] levels. At a low [Ca^{2+}] level (pCa = 5.0), both N98S-CaM and E46K-CaM showed higher [^{3}H]ryanodine binding levels than WT-CaM. Notably, E46K-CaM showed significantly higher [^{3}H]ryanodine binding levels than no CaM (Figure 5G), indicating E46K-CaM activates RyR2. The binding of N98S-CaM was comparable to that of no CaM, suggesting simple loss of inhibitory effect on RyR2. At a high [Ca^{2+}] level (pCa = 3.9), E46K-CaM showed similar [^{3}H]ryanodine binding levels as no CaM (Figure 5H), indicating completely no inhibitory effect on RyR2. In contrast, N98S-CaM showed similar inhibitory effect on RyR2 as WT-CaM. Thus, compared to N98S-CaM, E46K-CaM causes stronger facilitative effect on RyR2, leading to more severe arrhythmogenic features in both E46K iPSC-CMs and E46K RyR2-HEK293 cells.

E46K-CaM shows dramatically increased RyR2 affinity

Despite the facilitative effect of mutated CaM (E46K and N98S) on RyR2, it was still unclear how a single variant in one out of six CaM alleles caused severe arrhythmogenic features in mutant iPSC-CMs and severe clinical phenotypes in patients. The previous reports demonstrated that mutated CaMs exhibit higher RyR2 binding affinity than WT-CaM.[10] We therefore tested whether this is also the cause with E46K-CaM.

We employed a BLI strategy which measured real-time binding process between His-tagged FKBP12.6/RyR2 complex and CaMs (Figure S10) at low [Ca^{2+}] (30 nM) and high [Ca^{2+}] (100 μM) levels. The kinetic parameters such as the association rate (k_{on}), the dissociation rate (k_{off}), and the binding affinity constants ($K_D = k_{off}/k_{on}$) were calculated (Figure 6A and Figure S11). At a low [Ca^{2+}] level which mimics a physiological diastolic state in the cardiomyocytes,[32] E46K-CaM had much larger k_{on}

and slightly larger k_{off}, resulting in a tenfold decreased K_D compared to WT-CaM, indicating a tenfold higher binding affinity ($1/K_D$) to RyR2 (Figure 6B). In contrast, the RyR2 binding affinity of N98S-CaM increased twofold which caused by a larger k_{on} compared to WT-CaM (Figure 6B). At a high [Ca^{2+}] level, E46K-CaM had a twofold higher RyR2 binding affinity caused by a smaller k_{off} compared to WT-CaM, whereas no significant difference was found between N98S-CaM and WT-CaM (Figure 6C). These results indicate that the dramatically increased RyR2 binding affinity of E46K-CaM may account for the dominant effect of the variant, *CALM*2 p.E46K, in CPVT.

E46K-CaM does not change Ca^{2+} affinity or LTCC function

Ca^{2+}-binding affinity is critically important for CaM action and several CaM variants are known to affect Ca^{2+}-binding affinity.[8, 9] We therefore tested Ca^{2+}-binding affinity of E46K-CaM for N- and C-domains (Figure 6D).[22] E46K-CaM had no significant effects on the Ca^{2+} affinity of C- and N-domains. In contrast, N98S-CaM significantly decreased Ca^{2+} affinity of the C-domain (Figure 6E and F) as previously reported.[10] These results suggest that abnormal regulations by E46K-CaM is not related to Ca^{2+}-binding affinity.

The LTCC is also a major target of CaM and dysregulation of LTCC by mutated CaM is strongly linked with arrhythmias. We tested the effect of E46K-CaM on the LTCC function by measuring I_{CaL} in the single isolated Ctr and E46K iPSC-CMs (Figure S12A). There was no significant difference in time constants for the inactivation of I_{CaL} between Ctr and E46K (Figure S12B). These results indicate that the *CALM2* p.E46K does not affect Ca^{2+} affinity or the CDI of LTCC.

Drug testing in E46K iPSC-CMs

Considering the clinical pharmacotherapy in the two index patients, we evaluated the antiarrhythmic effects of nadolol and flecainide on the Ca^{2+} transients in E46K iPSC-CMs (Figure 7A). Drug concentrations were determined according to the therapeutic plasma concentrations (nadolol: 0.5-1.5 μM[33], flecainide: 0.5-2.4 μM[34]). Both nadolol and flecainide suppressed the abnormal Ca^{2+} waves in a dose-dependent manner (Figure 7B). Nadolol significantly decreased the Ca^{2+} transient amplitudes in a dose-dependent manner, in contrast, flecainide reversed the decreased Ca^{2+} transient amplitudes at 1 and 3 μM (Figure 7C). These results imply that both nadolol and flecainide have the potential in suppressing arrhythmogenicity caused by *CALM2* p.E46K, which is consistent with the clinical effects of both reagents in our patients.

Discussion

In 2012, Nyegaard et al. first reported CPVT cases caused by variants in the *CALM* gene (*CALM1* p.N54I and *CALM1* p.N98S),[7] and then functional studies were performed using heterologous expression systems,[10, 11] but never in human cardiomyocytes. In this study, we, for the first time, reported an iPSC-based study on CaM-related CPVT. Our patient-specific iPSC-CMs (E46K iPSC-CMs) showed severe SR Ca^{2+} leakage leading to EADs and DADs, which is consistent with the clinical phenotype of the patients. The biochemical analyses revealed that E46K-CaM had a strong facilitative effect on RyR2 due to the increased RyR2 binding affinity. In addition, the assessment of drug efficacy using the iPSC-CM model provided clinically useful findings.

The two patients carrying the novel variant, *CALM2* p.E46K, exhibited clear CPVT

phenotypes as exercise-induced bidirectional or polymorphic VTs (Figure 1D and E). Consistent with the CPVT phenotypes, our E46K iPSC-CMs recapitulated arrhythmogenic features such as abnormal depolarizations and abnormal Ca^{2+} waves, which occurred more frequently after adrenergic stimulation by isoproterenol treatment. Interestingly, unlike most CPVT-associated *RYR2* variants which mainly cause DADs in iPSC-CMs, E46K iPSC-CMs displayed both EADs and DADs (Figure 2). Previous studies showed that CPVT-associated *RYR2* variants resulted in "leaky" RyR2 channels, which promoted diastolic SR Ca^{2+} leak and DADs.[35] In this study, E46K iPSC-CMs showed early onset of abnormal Ca^{2+} waves (Figure S8) and severe SR Ca^{2+} leakage (Figure 4). These phenotypes were subsequently explained by the [^{3}H]ryanodine binding assay that E46K-CaM facilitated RyR2 channels at nearly all ranges of physiological [Ca^{2+}] levels (Figure 5F). Additionally, we found the unique cellular features of E46K iPSC-CMs resemble those of CMs with homozygous *CASQ2* variants that cause a severe autosomal-recessive form of CPVT.[36] In the homozygous *CASQ2*–R33Q knock-in mice myocytes, multiple short-coupled Ca^{2+} re-releases and afterdepolarizations occurred immediately after the peak of the Ca^{2+} transient (shown as EADs).[37] These evidences indicate that in E46K iPSC-CMs, SR Ca^{2+} leakage occurred at phase 3 and phase 4 of the cardiac cycle, which promoted EADs, DADs, and triggered activities. And thus, the novel variant, *CALM2* p.E46K was considered as highly arrhythmogenic.

The cellular mechanisms of arrhythmias caused by CaM variants are complex because CaM regulates multiple proteins.[2] Our biochemical analyses demonstrated that, the *CALM2* p.E46K variant did not affect CaM-Ca^{2+} affinity (Figure 6E and F) or the CDI of LTCC in iPSC-CMs (Figure S12). On the other hand, E46K-CaM failed to

inhibit RyR2 at all tested physiological [Ca^{2+}] levels, and rather activated RyR2 at low [Ca^{2+}] levels (Figure 5E to H). E46K-CaM also showed a significantly increased RyR2 binding affinity compared with WT-CaM (Figure 6B and C). The facilitative effect of E46K-CaM on RyR2 explained the higher frequency of Ca^{2+} oscillation, and lower $[Ca^{2+}]_{ER}$ threshold levels than WT-CaM in the RyR2-HEK293 cells (Figure 5A to D), and the robust arrhythmogenic features caused by Ca^{2+} leak in E46K iPSC-CMs. By combining cellular phenotypes and biochemical analyses, we concluded that, although E46K-CaM and WT-CaM are produced from 1 and 5 CaM alleles, respectively, in the patient's cardiomyocytes, E46K-CaM dominantly binds and facilitates RyR2 channels due to increased binding affinity, leading to Ca^{2+} leakage and arrhythmias. Therefore, our findings imply a highly arrhythmogenic effect of *CALM2* p.E46K which is consistent with the severe clinical CPVT phenotype in the patients carrying the variant.

Thus far, four CaM variants (p.N54I, p.N98S, p.A103V, and p.E46K) have been reported to be associated with CPVT (Table S6).[7, 11, 26] Intriguingly, *CALM2* p.N98S was also associated with LQTS,[25] due to the decreased Ca^{2+}-binding affinity in the CaM C-domain and impaired CDI of LTCC, as demonstrated in this study and other previous reports (Table S7).[8, 9] Regarding the arrhythmia phenotype, the variant, *CALM1* p.N54I is similar to *CALM2* p.E46K that the variant carriers do not exhibit LQTS and only show CPVT.[7] *CALM1* p.N54I was identified in multiple members of a large Swedish family and the carriers had arrhythmias with varied severity. In contrast, our probands carrying *CALM2* p.E46K, as a *de novo* variant, showed severe cardiac arrhythmia, PDA, and neurodevelopmental disorders (Table S6). In the functional analysis, E46K- and N54I-CaMs exhibited similar features, such as normal Ca^{2+} affinity, increased RyR2 affinity, and a facilitative effect on RyR2, which explains the pure CPVT phenotype in

the patients. However, E46K- and N54I-CaM showed differences in the binding affinity to RyR2. The previous study showed N54I-CaM had a twofold increased RyR2 binding affinity at a low [Ca^{2+}] level (30 nM) but similar affinity as WT-CaM at a high [Ca^{2+}] level (30 μM).[10] In contrast, our study showed that E46K-CaM exhibited a tenfold higher RyR2 binding affinity at a low [Ca^{2+}] level (30 nM) and a twofold higher affinity at a high [Ca^{2+}] level (100 μM) than WT-CaM (Figure 6B and C, and Table S7). Therefore, we speculate that *CALM2* p.E46K causes a higher severity of RyR2 dysfunction than *CALM1* p.N54I, which explains the differences in clinical performance.

Our results indicate that the increased RyR2 binding affinity of E46K-CaM plays an important role in the pathogenesis of CPVT caused by the *CALM2* p.E46K variant. A recent cryogenic electron microscopy (cryo-EM) study revealed a detailed structure of RyR2 complexed with apo-CaM or Ca^{2+}-CaM.[38] To address the mechanism of mutated CaM action at a structural level, we labeled the residues involved in CaM-related CPVT in two RyR2-CaM three-dimensional (3D) structures (RyR2 with apo-CaM and RyR2 with Ca^{2+}-CaM)[38] (Figure S13). N98 and A103, located in the CaM C-domain, hardly established any specific interactions with RyR2 amino acids. In contrast, E46 and N54, variants of which show similar phenotypes as discussed above, are relatively close to the adjacent RyR2 loops. Furthermore, negatively charged E46 residue in the apo-CaM N-domain is close to the positively charged residue, K2558 in the neighboring RyR2, where they may form an ionic interaction.[38] Therefore, we speculate the variant E46K (changed from negatively to positively charged) may change the interaction between RyR2 and CaM. However, further studies are needed to investigate the exact changes.

In addition to CPVT phenotypes, another interesting finding is that both patients

carrying *CALM2* p.E46K were diagnosed with neurodevelopmental disorders at an early age which were unrelated to any episodes of syncope or cardiac arrest. Recently, a cohort study showed that 34 of 421 (8%) CPVT patients with *RYR2* variants were diagnosed with a concomitant intellectual disability and showed more frequent supraventricular arrhythmias than patients without neurological phenotypes.[39, 40] In addition, most *RYR2* variants associated with an intellectual disability (16 out of 18 variants) induced a significantly higher caffeine response of RyR2 compared to the pure CPVT-related *RYR2* variants.[39] Similarly, gain-of-function variants in *CACNA1C* with severe dysfunction of LTCC cause syndromic LQTS type 8 (LQT8), Timothy syndrome, including prolonged QT intervals, autism spectrum disorders, and skeletal abnormalities.[41] On the other hand, variants that mildly modify the channel function have been reported to cause non-syndromic LQT8.[42] Considering CaM is highly expressed and regulates RyR2 in excitable neuronal cells,[43] and RyR2 plays an important role in Ca^{2+} homeostasis in the central nervous system,[44] it is reasonable to speculate that CaM variants may cause neurodevelopmental deficits. The present study showed that E46K-CaM facilitated RyR2 function and showed enhanced RyR2 binding affinity, which is higher than other CPVT-CaMs. These findings may explain why neurological complications appeared in both CPVT probands carrying *CALM2* p.E46K, but not in other reported CaM-related CPVT cases (Table S6). Moreover, our generated E46K iPSCs are useful in further studying the role of *CALM2* p.E46K in the regulation of neuronal cells.

Additionally, the E46K iPSC-CM model also provides a powerful platform to evaluate drug efficacy for CaM-related CPVT. β-blockers, inhibiting β-adrenergic mediated-activation of RyR2 channels, are the mainstay in the treatment of CPVT

patients.[45] Nadolol, a non-selective β-blocker, is often preferred, as it is described to decrease incidence and severity of ventricular arrhythmias in CPVT patients compared to other β-blockers.[46] However, we noticed that 4 out of 15 (26.7%) CaM-related CPVT patients treated with β-blockers experienced severe arrhythmic events, including cardiac arrest and sudden death, indicating insufficient protection (Table S6).[7] Since flecainide, a class Ic antiarrhythmic drug, has been used as an effective therapy in preventing arrhythmias in CPVT patients who are refractory to β-blockers therapies,[45] we examined the effects of nadolol and flecainide in E46K iPSC-CMs based on clinical settings[33, 34] (Figure 7). Both drugs efficiently alleviated abnormal Ca^{2+} waves in E46K iPSC-CMs which is consistent with the clinical response in the index patients. Interestingly, flecainide also rescued the decreased Ca^{2+} transient amplitude in E46K iPSC-CMs. Recent studies explained the efficacy of flecainide in CPVT with two mechanisms: direct blockade of RyR2 channels and inhibition of Na^{+} channels.[47] We speculated that in E46K iPSC-CMs, flecainide directly inhibited RyR2 channels and prevented Ca^{2+} leak, and therefore increased the SR Ca^{2+} storage, representing an increased Ca^{2+} transient amplitude. Meanwhile, inhibition of Na^{+} channels by flecainide can reduce the probability of afterdepolarizations. Thereby, we propose that flecainide can be an efficient therapy in CPVT in association with *CALM2* p.E46K.

In this study, there are potential limitations. In our cardiac differentiation protocol, we used metabolic purification, which was recently reported to induce electrophysiological changes similar to the phenotype in ischemic heart failure[48]. In addition, we cannot exclude the possibility that other undetected genetic factors except *CALM2* p.E46K might also contribute to the neurodevelopmental disorders.

Conclusion

In this study, we, for the first time, studied a CaM-related CPVT variant using iPSC-CM models. The iPSC-CMs bearing *CALM2* p.E46K showed robust arrhythmogenic features as E46K-CaM dominantly binds and facilitates RyR2. In addition, the assessment of drug efficacy in the patient's iPSC-CMs will contribute to precision medicine.

Author contributions:

J.G., T.Makiyama, Y.Yamamoto, N.K., and T.Murayama conceived and designed the work. J.G., T.Makiyama, Y.Yamamoto, T.Kobayashi, H.A., T.L.M., Y.W., A.K., T.I., T.A., H.H., H.K., H.M., M.N., K.C., M.F., K.N.,T.W. K.K. S.O. N.K., and T.Murayama acquired and analyzed the data. J.G., T.Makiyama, and T.Murayama wrote the original manuscript. Y.Yamamoto, T.Kobayashi, H.A., T.L.M., K.K., F.T., Y.Yoshida, N.M., K.W., S.O., N.K., T.S., M.H., and T.Kimura revised the manuscript. F.T., Y.Yoshida, N.M., K.W., T.S., M.H., and T.Kimura supervised the work. T.Makiyama and T.Murayama managed the project. All authors read and approved the revised manuscript.

Acknowledgements

We are grateful for Kyoko Yoshida for her technical assistance. The biolayer interferometry analysis was performed at the Medical Research Support Center, Graduate School of Medicine, Kyoto University.

Sources of Funding

This work was supported by grants from: JSPS KAKENHI (JP16K09499, JP19K08538 to T.Makiyama, JP19K17595 to Y.W., 20K11368 to T.Kobayashi, 19K07105, 22K06652 to N.K., and 19H03404, 22H02805 to T.Murayama), a grant from Japan Agency for Medical Research and Development (AMED) (JP20bm0804022, JP21bm0804022 to Y.Yoshida, JP18ek0109202 to S.O., JP19ek0109202 to N.K., JP20bm0104001 to K.W.， JP20am0101080 to T.Murayama and N.K. (support number 2621), and Translational Research Grant Seeds A164 to T.Makiyama), the Suzuken Memorial Foundation (T.Makiyama and T.Kimura), and Vehicle Racing Commemorative Foundation (6114, 6237, 6303 to T.Murayama).

Disclosures

Y.Yoshida owns stock in iPS Portal. All other authors declare no competing interests.

Supplemental Materials:

Supplemental Methods

Supplemental Tables I-VII

Supplemental Figures I-XIII

Reference [49]

References

1. Crivici A and Ikura M. Molecular and structural basis of target recognition by calmodulin. *Annu Rev Biophys Biomol Struct*. 1995;24:85-116.
2. Sorensen AB, Sondergaard MT and Overgaard MT. Calmodulin in a heartbeat. *FEBS J*. 2013;280:5511-32.
3. Fabiato A. Time and calcium dependence of activation and inactivation of calcium-induced release of calcium from the sarcoplasmic reticulum of a skinned canine cardiac Purkinje cell. *J Gen Physiol*. 1985;85:247-89.
4. Xu L and Meissner G. Mechanism of calmodulin inhibition of cardiac sarcoplasmic reticulum Ca2+ release channel (ryanodine receptor). *Biophys J*. 2004;86:797-804.
5. Crotti L, Johnson CN, Graf E, De Ferrari GM, Cuneo BF, Ovadia M, Papagiannis J, Feldkamp MD, Rathi SG, Kunic JD, et al. Calmodulin mutations associated with recurrent cardiac arrest in infants. *Circulation*. 2013;127:1009-17.
6. Reed GJ, Boczek NJ, Etheridge SP and Ackerman MJ. CALM3 mutation associated with long QT syndrome. *Heart Rhythm*. 2015;12:419-22.
7. Nyegaard M, Overgaard MT, Sondergaard MT, Vranas M, Behr ER, Hildebrandt LL, Lund J, Hedley PL, Camm AJ, Wettrell G, et al. Mutations in calmodulin cause ventricular tachycardia and sudden cardiac death. *Am J Hum Genet*. 2012;91:703-12.
8. Yamamoto Y, Makiyama T, Harita T, Sasaki K, Wuriyanghai Y, Hayano M, Nishiuchi S, Kohjitani H, Hirose S, Chen J, et al. Allele-specific ablation rescues electrophysiological abnormalities in a human iPS cell model of long-QT syndrome with a CALM2 mutation. *Hum Mol Genet*. 2017;26:1670-1677.
9. Limpitikul WB, Dick IE, Joshi-Mukherjee R, Overgaard MT, George AL, Jr. and Yue DT. Calmodulin mutations associated with long QT syndrome prevent inactivation of cardiac L-type Ca(2+) currents and promote proarrhythmic behavior in ventricular myocytes. *J Mol Cell Cardiol*. 2014;74:115-24.
10. Hwang HS, Nitu FR, Yang Y, Walweel K, Pereira L, Johnson CN, Faggioni M, Chazin WJ, Laver D, George AL, Jr., et al. Divergent regulation of ryanodine receptor 2 calcium release channels by arrhythmogenic human calmodulin missense mutants. *Circ Res*. 2014;114:1114-24.

11. Gomez-Hurtado N, Boczek NJ, Kryshtal DO, Johnson CN, Sun J, Nitu FR, Cornea RL, Chazin WJ, Calvert ML, Tester DJ, et al. Novel CPVT-Associated Calmodulin Mutation in CALM3 (CALM3-A103V) Activates Arrhythmogenic Ca Waves and Sparks. *Circ Arrhythm Electrophysiol*. 2016;9.
12. Fischer R, Koller M, Flura M, Mathews S, Strehler-Page MA, Krebs J, Penniston JT, Carafoli E and Strehler EE. Multiple divergent mRNAs code for a single human calmodulin. *J Biol Chem*. 1988;263:17055-62.
13. Hirose S, Murayama T, Tetsuo N, Hoshiai M, Kise H, Yoshinaga M, Aoki H, Fukuyama M, Wuriyanghai Y, Wada Y, et al. Loss-of-function mutations in cardiac ryanodine receptor channel cause various types of arrhythmias including long QT syndrome. *Europace*. 2022;24:497-510.
14. Maurissen TL and Woltjen K. Synergistic gene editing in human iPS cells via cell cycle and DNA repair modulation. *Nat Commun*. 2020;11:2876.
15. Takahashi K, Tanabe K, Ohnuki M, Narita M, Ichisaka T, Tomoda K and Yamanaka S. Induction of pluripotent stem cells from adult human fibroblasts by defined factors. *Cell*. 2007;131:861-72.
16. Yang L, Soonpaa MH, Adler ED, Roepke TK, Kattman SJ, Kennedy M, Henckaerts E, Bonham K, Abbott GW, Linden RM, et al. Human cardiovascular progenitor cells develop from a KDR+ embryonic-stem-cell-derived population. *Nature*. 2008;453:524-8.
17. Wuriyanghai Y, Makiyama T, Sasaki K, Kamakura T, Yamamoto Y, Hayano M, Harita T, Nishiuchi S, Chen J, Kohjitani H, et al. Complex aberrant splicing in the induced pluripotent stem cell-derived cardiomyocytes from a patient with long QT syndrome carrying KCNQ1-A344Aspl mutation. *Heart Rhythm*. 2018;15:1566-1574.
18. Kashiwa A, Makiyama T, Kohjitani H, Maurissen TL, Ishikawa T, Yamamoto Y, Wuriyanghai Y, Gao J, Huang H, Imamura T, et al. Disrupted Ca(V)1.2 selectivity causes overlapping long QT and Brugada syndrome phenotypes in the CACNA1C-E1115K iPS cell model. *Heart Rhythm*. 2022.
19. Uehara A, Murayama T, Yasukochi M, Fill M, Horie M, Okamoto T, Matsuura Y, Uehara K, Fujimoto T, Sakurai T, et al. Extensive Ca2+ leak through K4750Q cardiac ryanodine receptors caused by cytosolic and luminal Ca2+

hypersensitivity. *J Gen Physiol*. 2017;149:199-218.
20. Kurebayashi N, Murayama T, Ota R, Suzuki J, Kanemaru K, Kobayashi T, Ohno S, Horie M, Iino M, Yamashita F, et al. Cytosolic Ca2+-dependent Ca2+ release activity primarily determines the ER Ca2+ level in cells expressing the CPVT-linked mutant RYR2. *J Gen Physiol*. 2022;154.
21. Murayama T, Kurebayashi N, Oba T, Oyamada H, Oguchi K, Sakurai T and Ogawa Y. Role of amino-terminal half of the S4-S5 linker in type 1 ryanodine receptor (RyR1) channel gating. *J Biol Chem*. 2011;286:35571-35577.
22. VanScyoc WS, Sorensen BR, Rusinova E, Laws WR, Ross JB and Shea MA. Calcium binding to calmodulin mutants monitored by domain-specific intrinsic phenylalanine and tyrosine fluorescence. *Biophys J*. 2002;83:2767-80.
23. Richards S, Aziz N, Bale S, Bick D, Das S, Gastier-Foster J, Grody WW, Hegde M, Lyon E, Spector E, et al. Standards and guidelines for the interpretation of sequence variants: a joint consensus recommendation of the American College of Medical Genetics and Genomics and the Association for Molecular Pathology. *Genet Med*. 2015;17:405-24.
24. Nakagawa M, Koyanagi M, Tanabe K, Takahashi K, Ichisaka T, Aoi T, Okita K, Mochiduki Y, Takizawa N and Yamanaka S. Generation of induced pluripotent stem cells without Myc from mouse and human fibroblasts. *Nat Biotechnol*. 2008;26:101-6.
25. Makita N, Yagihara N, Crotti L, Johnson CN, Beckmann BM, Roh MS, Shigemizu D, Lichtner P, Ishikawa T, Aiba T, et al. Novel calmodulin mutations associated with congenital arrhythmia susceptibility. *Circ Cardiovasc Genet*. 2014;7:466-74.
26. Jimenez-Jaimez J, Palomino Doza J, Ortega A, Macias-Ruiz R, Perin F, Rodriguez-Vazquez del Rey MM, Ortiz-Genga M, Monserrat L, Barriales-Villa R, Blanca E, et al. Calmodulin 2 Mutation N98S Is Associated with Unexplained Cardiac Arrest in Infants Due to Low Clinical Penetrance Electrical Disorders. *PLoS One*. 2016;11:e0153851.
27. Tohyama S, Hattori F, Sano M, Hishiki T, Nagahata Y, Matsuura T, Hashimoto H, Suzuki T, Yamashita H, Satoh Y, et al. Distinct metabolic flow enables large-scale purification of mouse and human pluripotent stem cell-derived cardiomyocytes. *Cell Stem Cell*. 2013;12:127-37.

28. Parikh SS, Blackwell DJ, Gomez-Hurtado N, Frisk M, Wang L, Kim K, Dahl CP, Fiane A, Tonnessen T, Kryshtal DO, et al. Thyroid and Glucocorticoid Hormones Promote Functional T-Tubule Development in Human-Induced Pluripotent Stem Cell-Derived Cardiomyocytes. *Circ Res*. 2017;121:1323-1330.
29. Matsa E, Rajamohan D, Dick E, Young L, Mellor I, Staniforth A and Denning C. Drug evaluation in cardiomyocytes derived from human induced pluripotent stem cells carrying a long QT syndrome type 2 mutation. *Eur Heart J*. 2011;32:952-62.
30. Shannon TR, Ginsburg KS and Bers DM. Quantitative assessment of the SR Ca2+ leak-load relationship. *Circ Res*. 2002;91:594-600.
31. Chu A, Diaz-Munoz M, Hawkes MJ, Brush K and Hamilton SL. Ryanodine as a probe for the functional state of the skeletal muscle sarcoplasmic reticulum calcium release channel. *Mol Pharmacol*. 1990;37:735-41.
32. Wu X and Bers DM. Free and bound intracellular calmodulin measurements in cardiac myocytes. *Cell Calcium*. 2007;41:353-64.
33. Kalsoom S, Zamir A, Rehman AU, Ashraf W, Imran I, Saeed H, Majeed A, Alqahtani F and Rasool MF. Clinical pharmacokinetics of nadolol: A systematic review. *J Clin Pharm Ther*. 2022;47:1506-1516.
34. Conard GJ and Ober RE. Metabolism of flecainide. *Am J Cardiol*. 1984;53:41B-51B.
35. Sasaki K, Makiyama T, Yoshida Y, Wuriyanghai Y, Kamakura T, Nishiuchi S, Hayano M, Harita T, Yamamoto Y, Kohjitani H, et al. Patient-Specific Human Induced Pluripotent Stem Cell Model Assessed with Electrical Pacing Validates S107 as a Potential Therapeutic Agent for Catecholaminergic Polymorphic Ventricular Tachycardia. *PLoS One*. 2016;11:e0164795.
36. Lahat H, Pras E, Olender T, Avidan N, Ben-Asher E, Man O, Levy-Nissenbaum E, Khoury A, Lorber A, Goldman B, et al. A missense mutation in a highly conserved region of CASQ2 is associated with autosomal recessive catecholamine-induced polymorphic ventricular tachycardia in Bedouin families from Israel. *Am J Hum Genet*. 2001;69:1378-84.
37. Liu N, Denegri M, Dun W, Boncompagni S, Lodola F, Protasi F, Napolitano C, Boyden PA and Priori SG. Abnormal propagation of calcium waves and ultrastructural remodeling in recessive catecholaminergic polymorphic ventricular

tachycardia. *Circ Res*. 2013;113:142-52.
38. Gong D, Chi X, Wei J, Zhou G, Huang G, Zhang L, Wang R, Lei J, Chen SRW and Yan N. Modulation of cardiac ryanodine receptor 2 by calmodulin. *Nature*. 2019.
39. Lieve KVV, Verhagen JMA, Wei J, Bos JM, van der Werf C, Roses INF, Mancini GMS, Guo W, Wang R, van den Heuvel F, et al. Linking the heart and the brain: Neurodevelopmental disorders in patients with catecholaminergic polymorphic ventricular tachycardia. *Heart Rhythm*. 2019;16:220-228.
40. Sumitomo N, Sakurada H, Taniguchi K, Matsumura M, Abe O, Miyashita M, Kanamaru H, Karasawa K, Ayusawa M, Fukamizu S, et al. Association of atrial arrhythmia and sinus node dysfunction in patients with catecholaminergic polymorphic ventricular tachycardia. *Circ J*. 2007;71:1606-9.
41. Splawski I, Timothy KW, Sharpe LM, Decher N, Kumar P, Bloise R, Napolitano C, Schwartz PJ, Joseph RM, Condouris K, et al. Ca(V)1.2 calcium channel dysfunction causes a multisystem disorder including arrhythmia and autism. *Cell*. 2004;119:19-31.
42. Fukuyama M, Wang Q, Kato K, Ohno S, Ding WG, Toyoda F, Itoh H, Kimura H, Makiyama T, Ito M, et al. Long QT syndrome type 8: novel CACNA1C mutations causing QT prolongation and variant phenotypes. *Europace*. 2014;16:1828-37.
43. Sola C, Barron S, Tusell JM and Serratosa J. The Ca2+/calmodulin system in neuronal hyperexcitability. *Int J Biochem Cell Biol*. 2001;33:439-55.
44. Ziviani E, Lippi G, Bano D, Munarriz E, Guiducci S, Zoli M, Young KW and Nicotera P. Ryanodine receptor-2 upregulation and nicotine-mediated plasticity. *EMBO J*. 2011;30:194-204.
45. Priori SG, Wilde AA, Horie M, Cho Y, Behr ER, Berul C, Blom N, Brugada J, Chiang CE, Huikuri H, et al. HRS/EHRA/APHRS expert consensus statement on the diagnosis and management of patients with inherited primary arrhythmia syndromes: document endorsed by HRS, EHRA, and APHRS in May 2013 and by ACCF, AHA, PACES, and AEPC in June 2013. *Heart Rhythm*. 2013;10:1932-63.
46. Leren IS, Saberniak J, Majid E, Haland TF, Edvardsen T and Haugaa KH. Nadolol decreases the incidence and severity of ventricular arrhythmias during exercise stress testing compared with beta1-selective beta-blockers in patients with

781 catecholaminergic polymorphic ventricular tachycardia. *Heart Rhythm*.
782 2016;13:433-40.
783 47. Kryshtal DO, Blackwell DJ, Egly CL, Smith AN, Batiste SM, Johnston JN, Laver
784 DR and Knollmann BC. RYR2 Channel Inhibition Is the Principal Mechanism of
785 Flecainide Action in CPVT. *Circ Res*. 2021;128:321-331.
786 48. Davis J, Chouman A, Creech J, Monteiro da Rocha A, Ponce-Balbuena D, Jimenez
787 Vazquez EN, Nichols R, Lozhkin A, Madamanchi NR, Campbell KF, et al. In vitro
788 model of ischemic heart failure using human induced pluripotent stem cell-derived
789 cardiomyocytes. *JCI Insight*. 2021;6.
790 49. Simkin D, Papakis V, Bustos BI, Ambrosi CM, Ryan SJ, Baru V, Williams LA,
791 Dempsey GT, McManus OB, Landers JE, et al. Homozygous might be
792 hemizygous: CRISPR/Cas9 editing in iPSCs results in detrimental on-target
793 defects that escape standard quality controls. *Stem Cell Reports*. 2022;17:993-
794 1008.
795

Figure legends

Figure 1. Clinical characterization of the CPVT patients carrying *CALM2* p.E46K

(**A**) Pedigree of two CPVT affected patients from two unrelated families. Solid black indicates CPVT-affected patients. Plus sign indicates a carrier of a variant, *CALM2* p.E46K. Minus sign indicates a non-carrier of the variant. Probands are indicated with an arrow. (**B**) DNA sequence analysis of the control individual and the proband 1 from family 1. Red arrow indicates a heterozygous variant, c.136G>A, p.E46K, in *CALM2*. (**C**) Schematic model of calmodulin and Ca^{2+} binding loops in the N-domain (EF-I and II) and C-domain (EF-III and IV). Amino acids principally involved in the binding of Ca^{2+} ions are denoted with grey dotted lines. Color-substituted amino acids represent arrhythmia-associated residues in the EF-hands (circles) or in the linkers (squares); colors correspond to the associated phenotypes: catecholaminergic polymorphic ventricular tachycardia (CPVT, blue), long QT syndrome (LQTS, red), idiopathic ventricular fibrillation (IVF, green), and overlap phenotypes are shown in shaded color. The red dotted box indicates the novel CaM variant p.E46K. (**D** and **E**) Resting electrocardiograms (ECGs) (upper) and Holter ECG monitoring traces (lower) of the probands. (**D**) The ECG of the proband 1 was recorded at age 10 without medication (heart rate (HR) 47/min, QTc 381 msec). Polymorphic ventricular tachycardias (VTs) were recorded during exercise in the Holter ECG. (**E**) The ECG of the proband 2 was recorded at age 5 without medication (HR 55/min, QTc 400 msec). Bidirectional VTs were recorded during exercise in the Holter ECG. Rest ECGs of both probands exhibited sinus bradycardia and prominent U waves in the anterior leads, V_1 and V_2.

Figure 2. Optical action potential (AP) recordings of electrically stimulated

monolayer iPSC-CMs with CaM variants

(**A** and **B**) Representative AP traces recorded with FluoVolt from control (Ctr), *CALM2*-E46K, *CALM2*-E46K-correted isogenic control (E46K-Cor), and *CALM2*-N98S monolayer iPSC-derived cardiomyocytes (iPSC-CMs) at baseline (**A**) and after 100 nM isoproterenol treatment (**B**). Vertical bars indicate the timings of 1 Hz electrical stimulation. Red arrows indicate events of abnormal depolarizations. Blue triangles indicate arrhythmogenic triggered activities. (**C**) Frequency of abnormal depolarizations for 10 seconds at 1 Hz pacing. (**D**) AP durations (APDs) at 90% repolarization (APD_{90}) at baseline and after isoproterenol treatment. Data in (**C**) and (**D**) are from Ctr ($n = 32$), E46K ($n = 22$), E46K-Cor ($n = 16$), and N98S ($n = 14$). The data are shown as mean ± SEM. Comparisons between before and after isoproterenol treatment in each cell line were analyzed by two-tailed paired *t*-test ($^{\dagger\dagger\dagger}p < 0.001$ vs. baseline). Comparisons among multiple cell lines were analyzed by one-way ANOVA and post-hoc Tukey's test ($^{***}p < 0.001$).

Figure 3. Ca^{2+} transient recordings of electrically stimulated iPSC-CMs with CaM variants

(**A** and **B**) Representative Ca^{2+} transient traces recorded with Fluo-8 from control (Ctr), *CALM2*-E46K, *CALM2*-E46K-correted isogenic control (E46K-Cor), and *CALM2*-N98S single isolated iPSC-derived cardiomyocytes (iPSC-CMs) at baseline (**A**) and after 100 nM isoproterenol treatment (**B**). Vertical bars indicate the timings of 1 Hz electrical stimulation. Red arrows indicate events of abnormal Ca^{2+} waves. (**C**) Frequency of abnormal Ca^{2+} waves for 10 seconds at 1 Hz pacing. (**D**) Amplitudes of Ca^{2+} transients. The absolute fluorescence value (F) is normalized to the resting value of

fluorescence (F_0) and presented as $\Delta F/F_0 = (F-F_0)/F_0$. Data in (**C**) and (**D**) are from Ctr ($n = 32$), E46K ($n = 24$), E46K-Cor ($n = 20$), and N98S ($n = 18$). The data are shown as mean ± SEM. Comparisons between before and after isoproterenol treatment in each cell line were analyzed using two-tailed paired *t*-test ($^{\dagger}p < 0.05$, $^{\dagger\dagger\dagger}p < 0.001$ vs. baseline). Comparisons among multiple cell lines were analyzed by one-way ANOVA and post-hoc Tukey's test ($^{*}p < 0.05$, $^{**}p < 0.01$, $^{***}p < 0.001$).

Figure 4. Ca^{2+} homeostasis analysis in iPSC-CMs with CaM variants

(**A**) Representative traces of cytosolic Ca^{2+} homeostasis analysis in control (Ctr), *CALM2*-E46K, *CALM2*-E46K-correted isogenic control (E46K-Cor), and *CALM2*-N98S iPSC-derived cardiomyocytes (iPSC-CMs). Single isolated CMs loaded with Fluo-8 were firstly paced at 1 Hz in normal Tyrode's (NT) solution for 20 seconds and then exposed to Na^+, Ca^{2+} free solution and followed by treatment with 1 mM tetracaine (blue line) and 30 mM caffeine (orange line). The amount of the Ca^{2+} leakage from the sarcoplasmic reticulum (SR Ca^{2+} leak) is indicated by red arrows and the amount of the Ca^{2+} storage in SR (SR Ca^{2+} load) is indicated by brown arrows. The absolute fluorescence value (F) was normalized to the minimal fluorescence value (F_0) and presented as $\Delta F/F_0 = (F-F_0)/F_0$. (**B** and **C**) Normalized fluorescence intensity of SR Ca^{2+} leak (**B**) and SR Ca^{2+} load (**C**) (means ± SEM). Data are from Ctr ($n = 12$), E46K ($n = 10$), E46K-Cor ($n = 6$), and N98S ($n = 6$). Comparisons among multiple cell lines were analyzed by one-way ANOVA and post-hoc Tukey's test ($^{*}p < 0.05$, $^{**}p < 0.01$, $^{***}p < 0.001$).

Figure 5. Cytosolic and endoplasmic reticulum Ca^{2+} monitoring in HEK293 cells and [^{3}H]ryanodine binding assay

(**A**) Representative traces of Fluo-4 Ca^{2+} signals in RyR2-HEK293 cells exogenously expressing WT-, E46K- or N98S-CaM. (**B**) The frequency of Ca^{2+} oscillation. Data is from WT (n = 210), E46K (n = 210) and N98S (n = 210). (**C**) Representative traces of R-CEPIA1er signals in RyR2-HEK293 cells exogenously expressing various CaMs. Fluorescence signals in individual cells in (**A**) and (**C**) were determined in normal Krebs solution (blue line) and then in caffeine solution (orange box). The dashed line in the left trace in (**C**) mark the luminal Ca^{2+} thresholds. (**D**) The threshold level of $[Ca^{2+}]_{ER}$. Data is from WT (n = 97), E46K (n = 148), and N98S (n = 117). Data in (**B**) and (**D**) are shown as box and whisker plots (the center line denotes the median; the box contains the 25% to 75% of dataset and whiskers mark values from minimal to maximum). (**E**) Ca^{2+}-dependent [^{3}H]ryanodine binding of RyR2 with or without 1 μM WT-CaM. (**F**) The effect of WT-CaM and mutated CaMs (E46K and N98S) on Ca^{2+}-dependent [^{3}H]ryanodine binding. (**G**) and (**H**) [^{3}H]ryanodine binding ratio without CaM or with 1 μM various CaMs at pCa = 5.0 (**G**) and pCa = 3.9 (**H**). Data in (**E**) to (**H**) are from no CaM (n = 4) and 1 μM WT/E46K/N98S CaMs (n = 6, respectively). Comparisons among multiple groups in (**B**), (**D**), (**F**), (**G**) and (**H**) were analyzed by one-way ANOVA and post-hoc Tukey's test (*p < 0.05, **p < 0.01, ***p < 0.001; $^{‡}p$ < 0.05 (E46K vs. WT), $^{§}p$ < 0.05 (E46K vs. N98S), and $^{‖}p$ < 0.05 (N98S vs. WT). Comparisons between two groups in (**E**) was analyzed using two-tailed no-paired t-test ($^{†}p$ < 0.05).

Figure 6. Binding affinity of mutated CaMs to RyR2 and Ca^{2+}

(**A**) A schematic of real-time CaM-RyR2 binding affinity analysis using bio-layer interferometry. Changes in the number of molecules bound to the biosensor tip induce a

888 shift in the wavelength of the interference pattern of reflected white light. (**B**) and (**C**)
889 Binding kinetics parameters between CaM and RyR2 at low [Ca^{2+}] as 30 nM (**B**) and
890 high [Ca^{2+}] as 100 μM (**C**). Parameters describing CaM-RyR2 real-time binding, such
891 as association rate (k_{on}) (left), dissociation rate (k_{off}) (middle), and CaM-RyR2 binding
892 affinity constants (K_D) (right) are shown as means ± SEM (n = 5 in each group).
893 Comparisons among multiple groups were analyzed by one-way ANOVA and post-hoc
894 Tukey's test (*p < 0.05, **p < 0.01, ***p < 0.001). (**D**) A schematic of Ca^{2+}-CaM
895 affinity analysis by monitoring domain-specific intrinsic phenylalanine (Phe) and
896 tyrosine (Tyr) fluorescence (Fluor). (**E**) Typical Ca^{2+} titration curves for the CaM N-
897 domain (left) and C-domain (right). (**F**) Dissociation constants for Ca^{2+}-CaM binding
898 (K_D, in μmol/L) in the CaM N-domain (left) and C-domain (right). Values are averages
899 of 3 independent experiments, and error was determined by analysis of the curve fits.
900 Comparisons among multiple groups were analyzed by one-way ANOVA and post-hoc
901 Tukey's test (***p < 0.001).

902 **Figure 7. Drug testing in *CALM2*-E46K iPSC-CMs**

903 (**A**) Representative Ca^{2+} transient traces recorded from single isolated *CALM2*-E46K
904 iPSC-derived cardiomyocytes (iPSC-CMs) in a series of 4 consecutive Ca^{2+} transient
905 recordings performed at baseline and applied with 1, 3, and 10 μM nadolol (left) or
906 flecainide (right). Vertical bars indicate the timings of 1 Hz electrical stimulation. Red
907 arrows indicate events of abnormal Ca^{2+} waves. (**B**) Frequency of abnormal Ca^{2+} waves
908 for 10 seconds at 1 Hz pacing. (**C**) Amplitudes of Ca^{2+} transients. The absolute
909 fluorescence value (F) was normalized to the resting value of fluorescence (F_0) and
910 presented as $\Delta F/F_0 = (F-F_0)/F_0$. Data in (**B**) and (**C**) are from *CALM2*-E46K iPSC-CMs

911 treated with each drug ($n = 10$, respectively). Comparisons among different doses of the
912 drug treatment were analyzed by one-way ANOVA and post-hoc Tukey's test (*$p <$
913 0.05, **$p < 0.01$, ***$p < 0.001$).

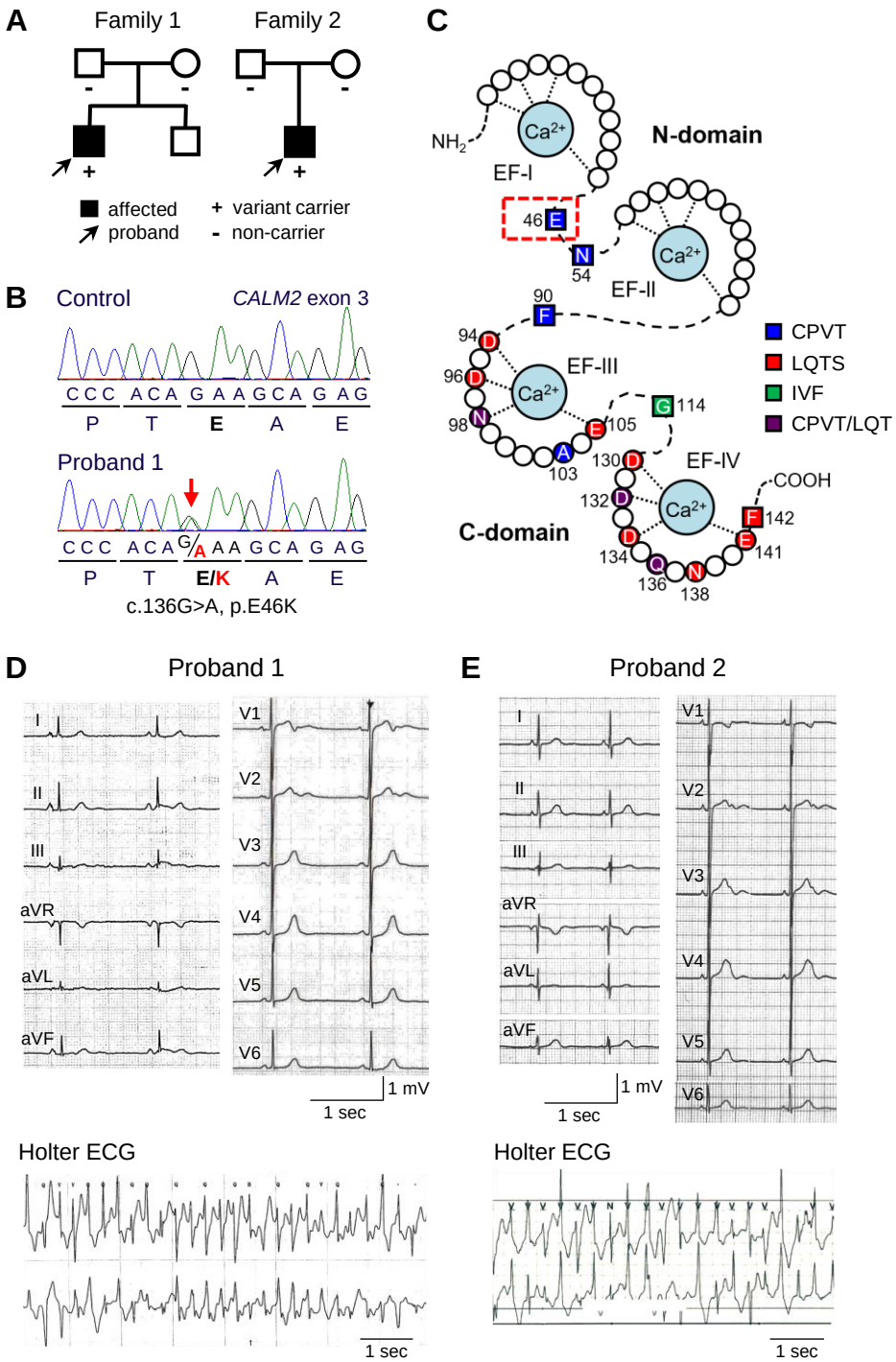
A
Family 1
Family 2
affected
proband
variant carrier
non-carrier
B
Control
CALM2 exon 3
C C C A C A G A A G C A G A G
P T E A E
Proband 1
C C C A C A G/A A A G C A G A G
P T E/K A E
c.136G>A, p.E46K
C
NH2
Ca2+
N-domain
EF-I
46 E
N 54
EF-II
90 F
94 D
96 D
98 N
EF-III
G 114
E 105
A 103
130 D
132 D
D 134
Q 136
N 138
EF-IV
COOH
F 142
E 141
C-domain
CPVT
LQTS
IVF
CPVT/LQT
D
Proband 1
I
II
III
aVR
aVL
aVF
V1
V2
V3
V4
V5
V6
1 mV
1 sec
Holter ECG
1 sec
E
Proband 2
I
II
III
aVR
aVL
aVF
V1
V2
V3
V4
V5
V6
1 mV
1 sec
Holter ECG
1 sec

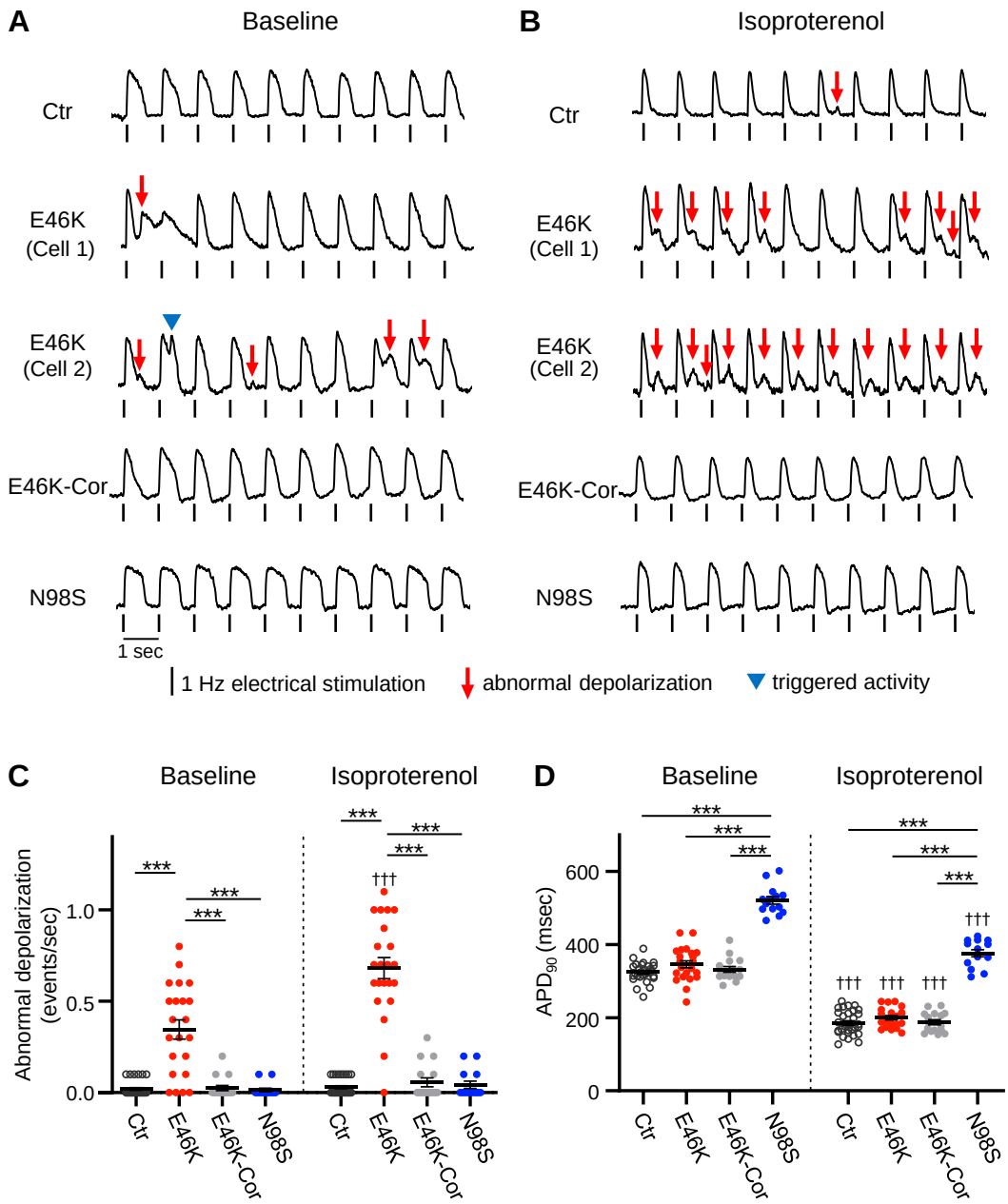
A
Baseline
B
Isoproterenol
Ctr
E46K
(Cell 1)
E46K
(Cell 2)
E46K-Cor
N98S
1 sec
1 Hz electrical stimulation
abnormal depolarization
triggered activity
C
Baseline
Isoproterenol
Abnormal depolarization
(events/sec)
1.0
0.5
0.0
***
†††
Ctr
E46K
E46K-Cor
N98S
D
Baseline
Isoproterenol
APD90 (msec)
600
400
200
0
***
†††

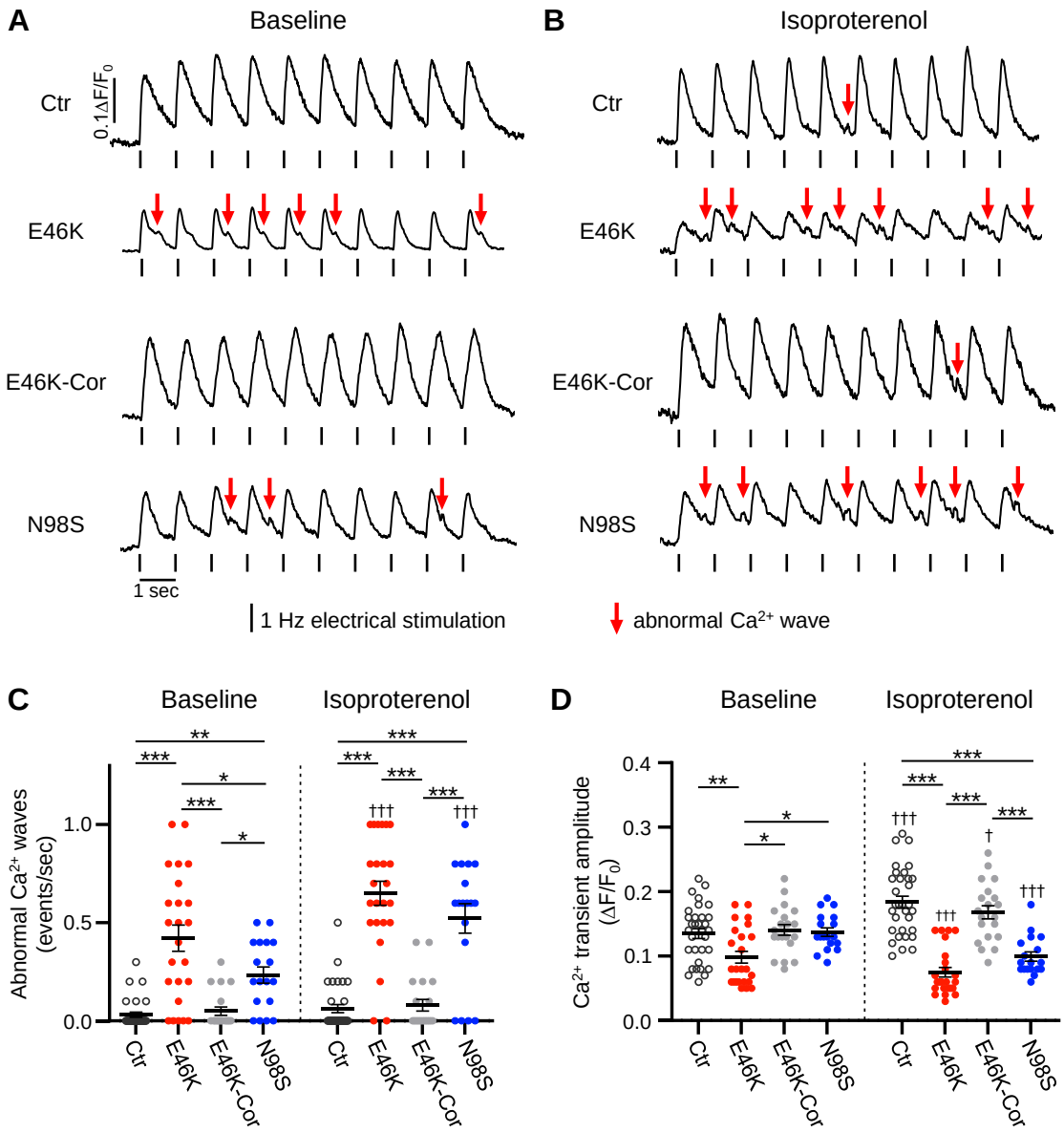
A
Baseline
Ctr
0.1ΔF/F0
E46K
E46K-Cor
N98S
1 sec
1 Hz electrical stimulation
B
Isoproterenol
Ctr
E46K
E46K-Cor
N98S
abnormal Ca2+ wave
C
Baseline
Isoproterenol
Abnormal Ca2+ waves (events/sec)
1.0
0.5
0.0
Ctr
E46K
E46K-Cor
N98S
D
Baseline
Isoproterenol
Ca2+ transient amplitude (ΔF/F0)
0.4
0.3
0.2
0.1
0.0
Ctr
E46K
E46K-Cor
N98S

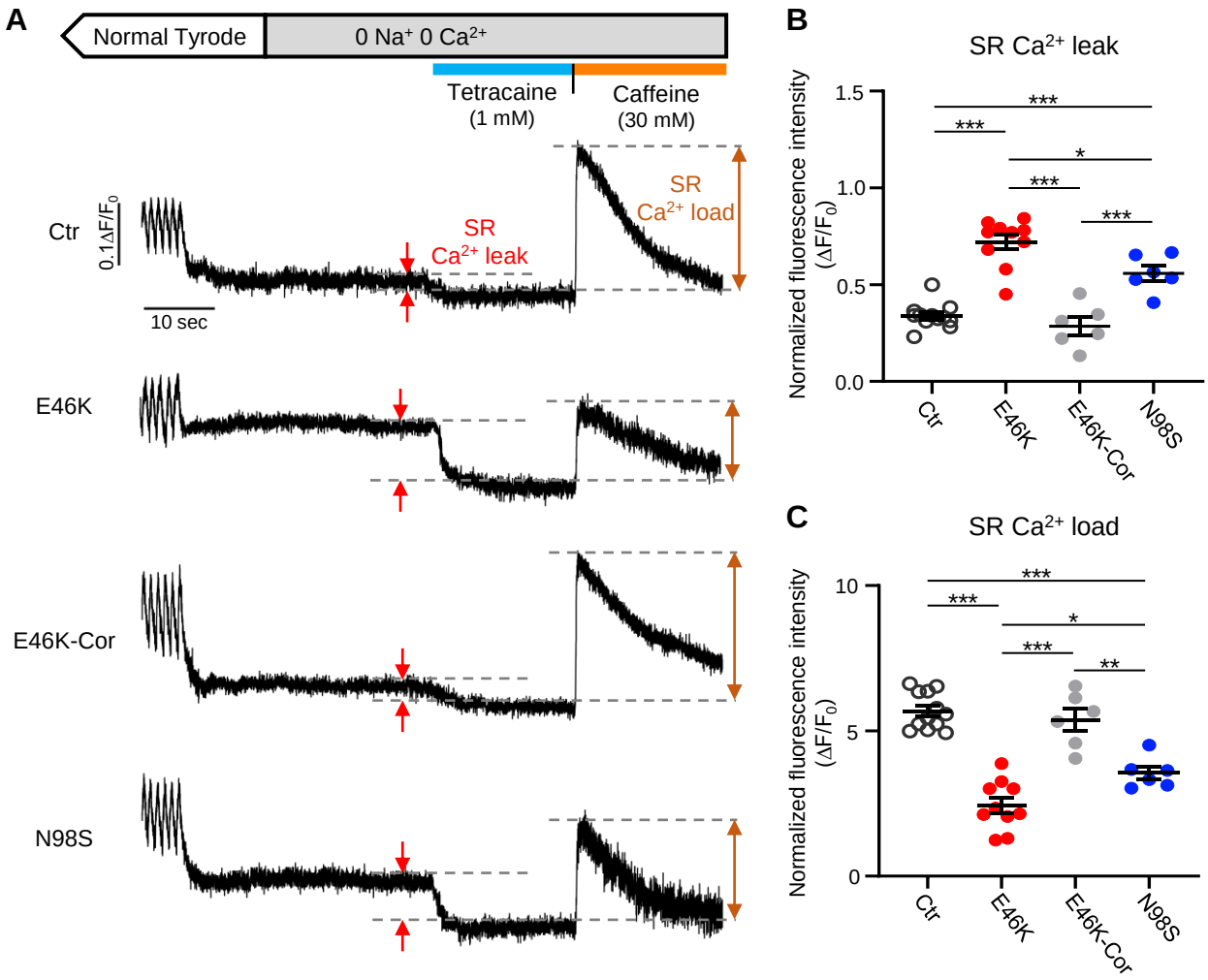
A
Normal Tyrode
0 Na+ 0 Ca2+
Tetracaine
(1 mM)
Caffeine
(30 mM)
Ctr
0.1ΔF/F0
SR
Ca2+ leak
SR
Ca2+ load
10 sec
E46K
E46K-Cor
N98S
B
SR Ca2+ leak
Normalized fluorescence intensity
(ΔF/F0)
1.5
1.0
0.5
0.0
***
***
*
***
***
Ctr
E46K
E46K-Cor
N98S
C
SR Ca2+ load
Normalized fluorescence intensity
(ΔF/F0)
10
5
0
***
***
*
***
**
Ctr
E46K
E46K-Cor
N98S

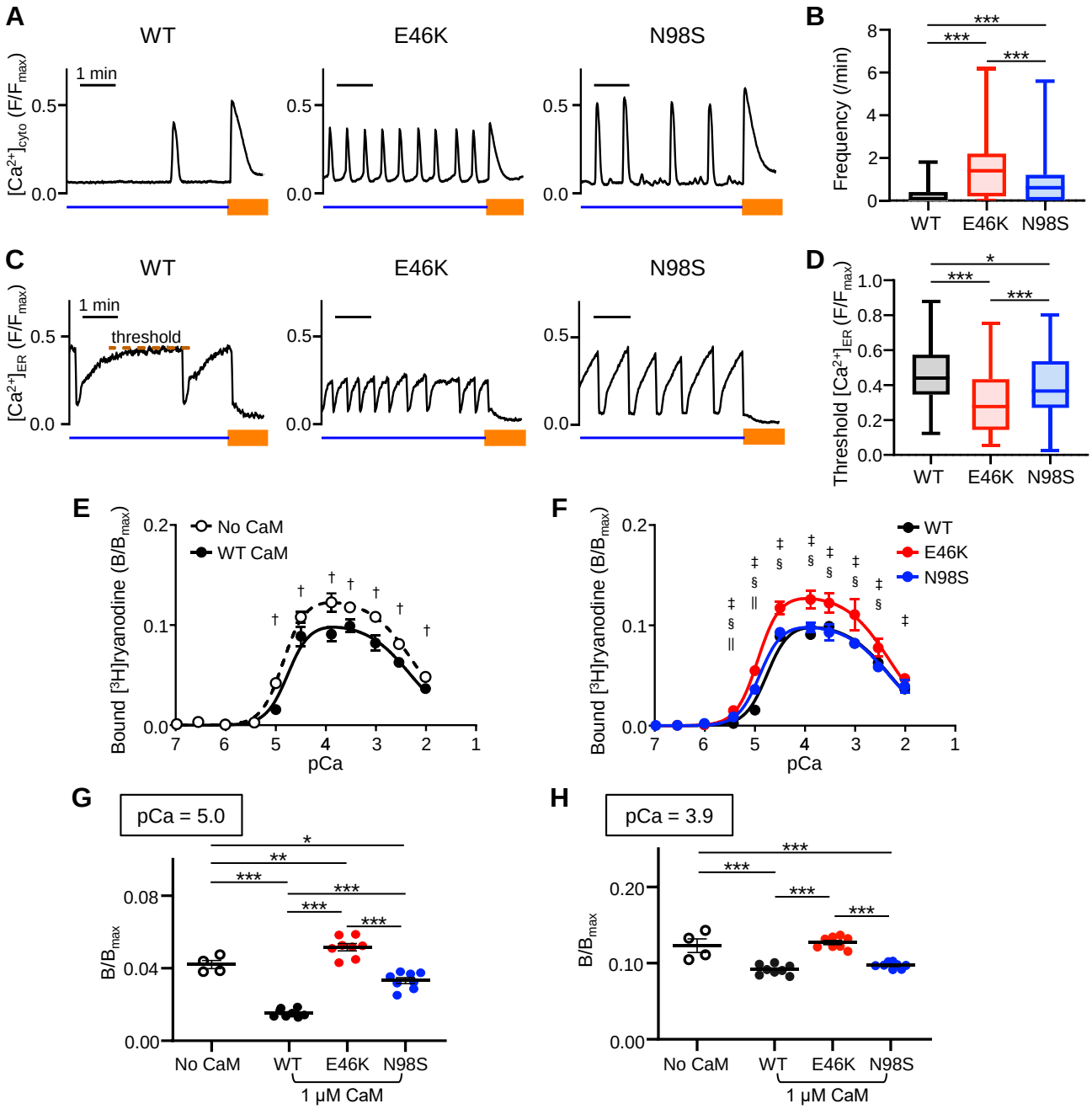
A
WT
E46K
N98S
1 min
[Ca2+]cyto (F/Fmax)
0.5
0.0
B
Frequency (/min)
***
WT
E46K
N98S
C
threshold
[Ca2+]ER (F/Fmax)
D
Threshold [Ca2+]ER (F/Fmax)
*
E
No CaM
WT CaM
Bound [3H]ryanodine (B/Bmax)
pCa
F
G
pCa = 5.0
B/Bmax
No CaM
1 µM CaM
H
pCa = 3.9

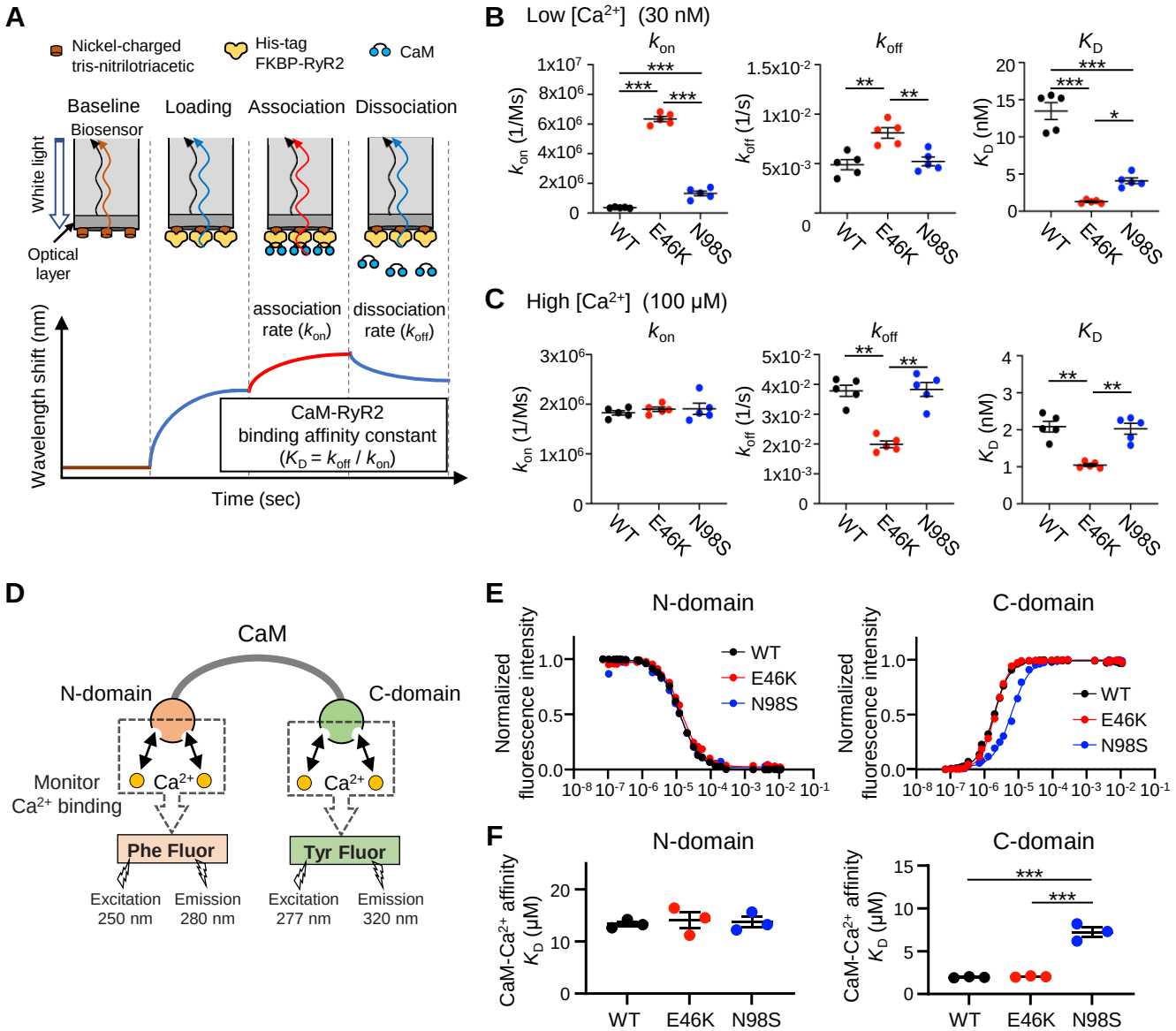
A
Nickel-charged tris-nitrilotriacetic
His-tag FKBP-RyR2
CaM
Baseline
Biosensor
Loading
Association
Dissociation
White light
Optical layer
association rate (k_{on})
dissociation rate (k_{off})
Wavelength shift (nm)
CaM-RyR2 binding affinity constant ($K_D = k_{off} / k_{on}$)
Time (sec)
B
Low [Ca2+] (30 nM)
k_{on}
k_{off}
K_D
k_{on} (1/Ms)
k_{off} (1/s)
K_D (nM)
WT
E46K
N98S
C
High [Ca2+] (100 μM)
D
CaM
N-domain
C-domain
Monitor Ca2+ binding
Ca2+
Phe Fluor
Tyr Fluor
Excitation 250 nm
Emission 280 nm
Excitation 277 nm
Emission 320 nm
E
N-domain
C-domain
Normalized fluorescence intensity
F
CaM-Ca2+ affinity K_D (μM)

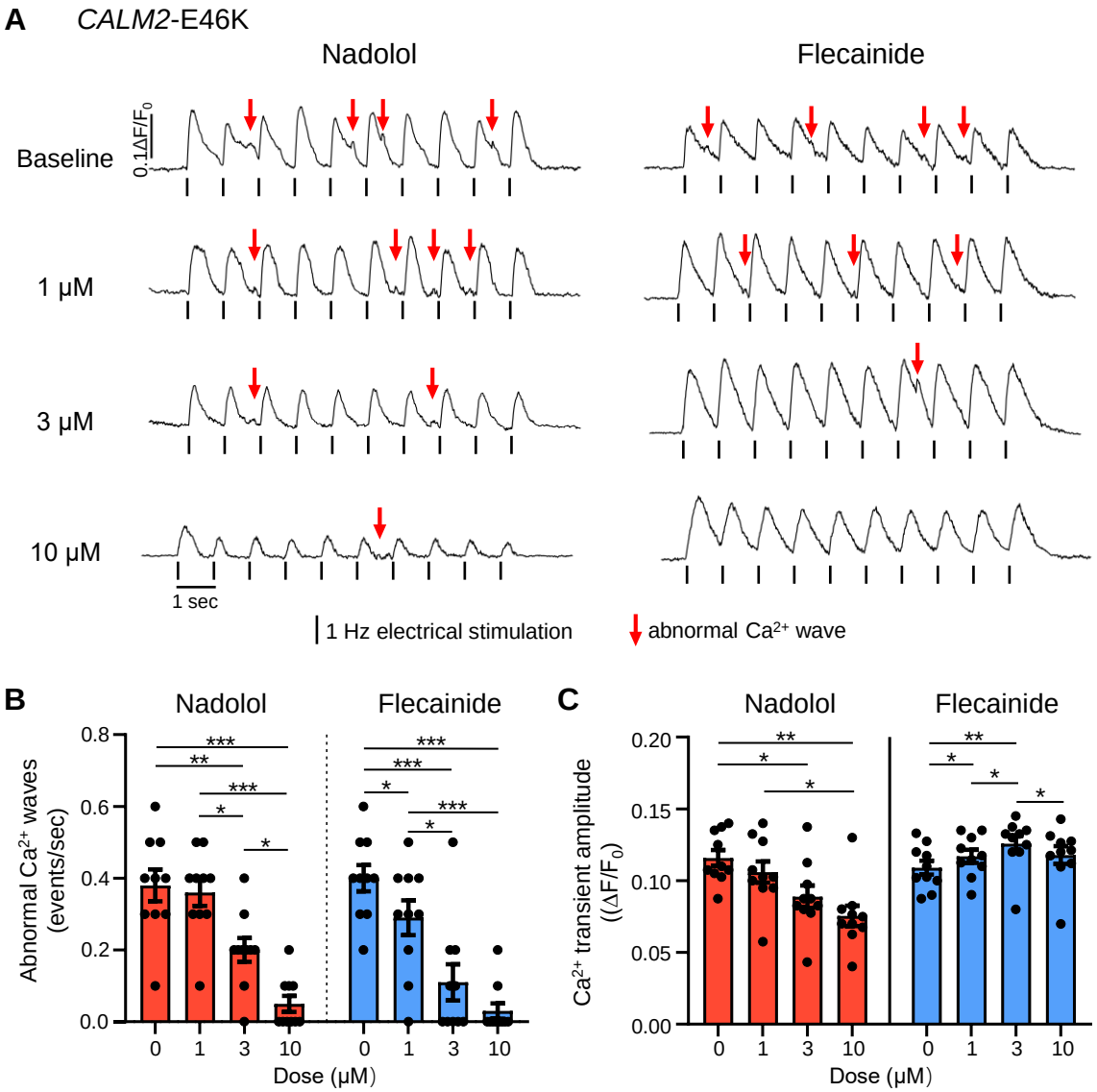
A
CALM2-E46K
Nadolol
Flecainide
Baseline
1 μM
3 μM
10 μM
0.1ΔF/F0
1 sec
1 Hz electrical stimulation
abnormal Ca2+ wave
B
Nadolol
Flecainide
Abnormal Ca2+ waves (events/sec)
Dose (μM)
C
Nadolol
Flecainide
Ca2+ transient amplitude ((ΔF/F0)
Dose (μM)

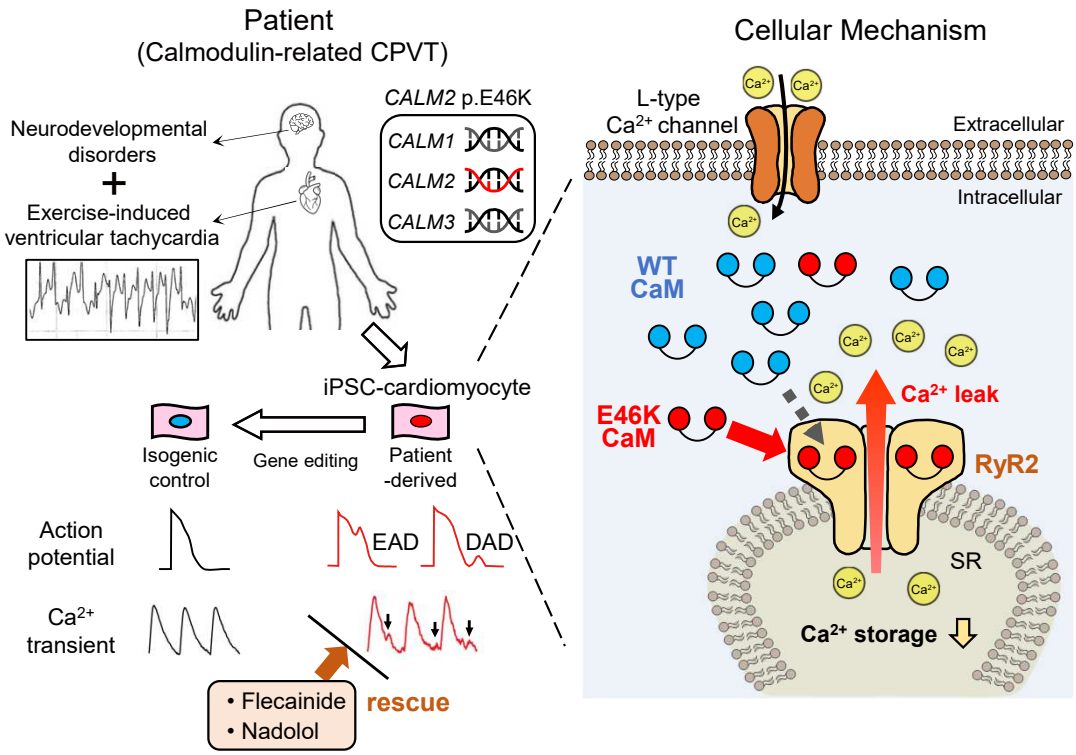
Patient
(Calmodulin-related CPVT)
Neurodevelopmental disorders
+
Exercise-induced ventricular tachycardia
CALM2 p.E46K
CALM1
CALM2
CALM3
iPSC-cardiomyocyte
Isogenic control
Gene editing
Patient -derived
Action potential
EAD
DAD
Ca2+ transient
• Flecainide
• Nadolol
rescue
Cellular Mechanism
L-type Ca2+ channel
Extracellular
Intracellular
WT CaM
E46K CaM
Ca2+ leak
RyR2
SR
Ca2+ storage

SUPPLEMENTAL MATERIAL

Supplemental Methods

Generation of patient-derived induced pluripotent stem cells (iPSCs) bearing *CALM2* p.E46K

This study was approved by the ethical committee of human research at Kyoto University (Kyoto, Japan). The study conformed to the principles of the Declaration of Helsinki and written informed consents were obtained from all the participants. The patient-specific iPSC clones were generated by reprogramming of peripheral blood mononuclear cells as previously described.[15] As a control, 201B7 iPSC line generated from a healthy individual was used in this study.[15, 24] We also used a previously established iPSC line from a patient with long QT syndrome bearing *CALM2* p.N98S,[8, 25] which was also reported in catecholaminergic polymorphic ventricular tachycardia (CPVT) patients.[26]

Maintenance of iPSCs

1. Feeder-dependent (on-feeder) culture

iPSCs were maintained on a mitomycin C-treated SNL feeder layer in Primate ES cell medium (ReproCELL, Tokyo, Japan) in 6-well plates at 37°C and 5% CO_2.[16] The cells were replated at a density of 0.5×10^6 cells per six-well plate for each passaging. The iPSCs cultured with the on-feeder method were used for cardiac differentiation in this study.

2. Feeder-free culture

iPSCs were maintained in 6-well plates coated with 0.5 mg/mL iMatrix-511 silk

(Matrixome, Osaka, Japan) in mTeSR Plus medium (STEMCELL Technologies, Vancouver, Canada) at 37°C and 5% CO_2. The cells were replated at a density of 0.3×10^6 cells per six-well plate for each passaging. The iPSCs cultured with feeder-free method were used for immunocytochemistry and generation of a gene-corrected isogenic iPSC line.

Deoxyribonucleic acid (DNA) sequencing

Genomic DNA was isolated from the peripheral white blood cells of the patients and their family members. Genetic analyses were performed through targeted gene sequencing of 60 genes (Table S1) using the MiSeq System (Illumina, CA, USA). Detected variants were confirmed through Sanger sequencing. The variant was evaluated by comparing with the human genomic variation databases (gnomAD, ExAC, HGVD, and iJGVD).[13] In Sanger sequencing, purified DNA was amplified with specific primers and analyzed with Genetic Analyzer 3130 and Big Dye Terminator v3.1 (Thermo Fisher Scientific, Waltham, MA, USA). The information of the primers is described in Table S2.

Karyotyping and immunocytochemistry in iPSCs

Chromosomal Q-band analysis was performed by Trans Chromosomics (Tottori, Japan). The samples were prepared as follows: feeder free iPSCs at 70-90% confluence were incubated with 0.25 μg/ml Metaphase Arresting Solution (Funakoshi, Tokyo, Japan) and 1/10000 Chromosome Resolution Additive (Funakoshi) for 1.5 hours at 37°C. Then the iPSCs were dispersed with Accumax (Nacalai Tesque, Kyoto, Japan) and treated with hypotonic solution (0.075 M KCl), and fixed with cold methanol-acetic acid solution (3:1).

The pluripotency of established iPSCs was assessed using immunostaining.[18] iPSC

colonies were fixed in 4% paraformaldehyde (Nacalai Tesque) and permeabilized in 0.2% Triton X-100 (Nacalai Tesque). The samples were stained with the following primary antibodies: mouse monoclonal anti-OCT3/4 (1:50; Santa Cruz Biotechnology, Dallas, TX, USA), mouse monoclonal anti-SSEA4 (1:200; Santa Cruz Biotechnology), and mouse monoclonal anti-TRA 1-60 (1:200; Santa Cruz Biotechnology). The secondary antibody was donkey anti-mouse Alexafluor 488 (1:1000; Thermo Fisher Scientific). The nuclei were stained with DAPI (1:2000; FUJIFILM Wako pure Chemical industries, Osaka, Japan). The specimens were observed under a fluorescence microscope (Biozero BZ-9000; Keyence, Osaka, Japan).

Generation of a gene-corrected isogenic iPSC line with the patient-derived iPSCs

An isogenic control iPSC line was created by correcting the *CALM2* c.136G>A, p.E46K in the patient-derived iPSC line using the CRISPR/Cas9-based gene editing strategy as previously described[14] (Figure S2A). We designed a synthetic CRISPR RNA (crRNA; Integrated DNA Technologies (IDT), Skokie, IL, USA) to target the mutation site and a single-stranded oligonucleotide (ssODN; IDT) as a repair template. The detail sequences of crRNA and ssODN are shown in Table S2. A ribonucleoprotein (RNP) complex was prepared by mixing the Alt-R Cas9 Nuclease 3NLS and the crRNA: tracrRNA duplex (IDT). The RNP complex and the repair template oligo were introduced into 1.0×10^6 iPSCs by electroporation using the NEPA21 electroporator (Nepa Gene, Ichikawa, Japan). Electroporated cells were maintained for 1 week and then were dispersed with Accumax into single cells. Single colonies were picked and screened by polymerase chain reaction (PCR). Sanger sequencing was used to confirm the sequence of the targeted site. Two gene-corrected isogenic control iPSC clones were generated and used in this study.

Analysis of on-target and off-target effects in CRISPR/Cas9-based gene editing

The CRISPR/Cas9 on-target and off-target analyses were performed as previously described.[49] The genomic DNA was extracted from the *CALM2* p.E46K patient-derived iPSC clones and the gene-corrected isogenic iPSC clones. To analyze the on-target unintended genome modification, PCR was performed to amplify 2760 base pairs including the CRISPR/Cas9 target site. Sager sequencing was done every ~400 bases along the amplified PCR fragment to identify any heterozygous single nucleotide polymorphism (Figure S2). Potential off-target regions with homology to the guide RNA sequence were predicted by the CRISPR/Cas9 guide RNA design checker (IDT) and the top 3 potential off-target regions (Table S4) were analyzed by Sanger sequencing. All the PCR and sequencing primer sequences are shown in Table S2.

iPSC cardiac differentiation, purification, and maturation

iPSCs were differentiated into cardiomyocytes (CMs) using an embryoid body (EB) differentiating system[16], and the iPSC-CMs were purified in a glucose-depleted lactate medium during Day 14 to 20, as previously described.[27] Further maturation of CMs was performed using media supplemented with 100 nmol/L triiodo-L-thyronine (T3; Nacalai Tesque) and 1000 nmol/L dexamethasone (Dex; Nacalai Tesque) during Day 21 to 35, as previously described.[28] CMs were analyzed 5-6 weeks after cardiac differentiation. More than two independent clones of each cell line were used in each experiment. All experimental data were collected from at least 3 independent differentiations.

Immunocytochemistry in iPSC-CMs

iPSC-CMs (5-6 weeks old) were dispersed with collagenase B (Roche, Basel, Switzerland) and Trypsin EDTA into single cells and plated onto glass coverslips. The

iPSC-CMs were fixed in 4% paraformaldehyde and permeabilized in 0.2% Triton X-100. The samples were stained with the following primary antibodies: mouse polyclonal anti-cardiac troponin T (cTnT) (1:200; Santa Cruz Biotechnology), mouse monoclonal anti-atrial myosin light chain 2 (MLC2a) (1:200; Santa Cruz Biotechnology), and rabbit polyclonal anti-ventricular myosin light chain 2 (MLC2v) (1:100; Santa Cruz Biotechnology). The secondary antibodies are donkey anti-mouse Alexafluor 594 (1:500; Thermo Fisher Scientific) and donkey anti-rabbit Alexafluor 488 (1:500; Thermo Fisher Scientific). The nuclei were stained with DAPI (1:2000).

Real-time quantitative reverse transcription PCR

Total RNA was extracted from 40-day-old iPSC-CMs using TRIzol Reagent (Thermo Fisher Scientific). The RNA was treated with a TURBO DNA-free Kit (Thermo Fisher Scientific) and transcribed into complementary DNA (cDNA) using Transcriptor First Strand cDNA Synthesis Kit (Roche). Quantitative PCR (qPCR) was performed with a THUNDERBIRD SYBR qPCR Mix (TOYOBO, Osaka, Japan). The expression of the genes was normalized relative to *GAPDH* and assessed the comparative change using the threshold cycle (ΔC_T) method. The list of primers is described in Table S2.

Optical recording of action potentials (APs) and Ca^{2+} transients in iPSC-CMs

1. Optical AP recording

Spontaneously beating CMs (5-6 weeks old) differentiated from iPSCs were dispersed with collagenase B and Trypsin EDTA. They were then cultured on a 96-well-plate coated with 4 μL of Corning Matrigel Growth Factor Reduced (GFR) Basement Membrane (Corning, New York, USA) with a total amount of 3×10^4 cells. The iPSC-CM monolayers were maintained in a medium containing DMEM/F12 (Nacalai Tesque) with 2% fetal bovine serum (Sigma-Aldrich, St. Louis, MO, USA) for 5-7

days before the recording. After washing with a normal Tyrode's (NT) solution containing (in mmol/L) 140 NaCl, 0.33 NaH_2PO_4, 5.4 KCl, 1.8 $CaCl_2$, 0.5 $MgCl_2$, 5.0 HEPES, and 5.5 D-Glucose, the iPSC-CM monolayers were loaded with a membrane potential dye, FluoVolt (F10448, Thermo Fisher Scientific), which was immersed in NT solution for 30 minutes (min) at 37°C in 5% CO_2, and then the medium was replaced with NT solution. Optical AP data was acquired using a microscope (Nikon Eclipse Ti2; Nikon, Tokyo, Japan) equipped with a 100×100 pixels CMOS fast camera system (MiCAM03-N256; Brainvision, Tokyo, Japan) at 40% LED power (X-Cite FIRE, Excelitas Technologies, Waltham, MA, USA), and was developed with an image processing software (BV_Ana and BV_Workbench; Brainvision) for baseline correction and colored visualization. The recordings were performed at 36.0 ± 1.0 °C with the following protocol: 5 secs without pacing followed by 10 secs with 1 Hz electrical field stimulation (Electronic Stimulator SEN-3301, Isolater SS-203JMG; Nihon Kohden, Tokyo, Japan), and another 5 secs without pacing. The iPSC-CMs were stimulated at 1 Hz with 4 msec depolarizing pulses at 12 V using platinum electrodes (Inter Medical, Nagoya, Japan), with an interelectrode distance of 4 mm. To analyze CMs with the same beating rate, CMs with self-beating faster than 1 Hz were excluded from the analysis. Abnormal depolarizations were defined as non-stimulated positive (depolarizing) oscillations (at least 3% of the full-wave amplitude) occurring during phase 2 to 4 of the AP. Arrhythmogenic triggered activities were defined as the full AP waves caused by abnormal depolarizations. AP durations (APDs) were calculated in the waves without abnormal depolarizations or triggered activities and were presented as APDs at 50% and 90% of the repolarizations (APD_{50} and APD_{90}). A solution containing 100 nM isoproterenol (LKT Laboratories, Saint Paul, MN, USA) was prepared immediately before the experiment, applied to the cells for

5 min, and the recordings were performed in the same way as the baseline condition. The optical AP maps were analyzed to calculate the conduction velocities using BV_Ana software.

2. Ca^{2+} transient recording

iPSC-CMs (5-6 weeks old) were dispersed with collagenase B and Trypsin EDTA into single cells and plated onto glass coverslips. After 5-7 days of maintenance in the medium containing DMEM/F12 with 2% FBS, the single isolated iPSC-CMs were loaded with 2 μmol/L Fluo-8 (AAT Bioquest, Sunnyvale, CA, USA) that was immersed in the medium described above. After 30 min of incubation at 37°C in 5% CO_2, the medium was replaced with NT solution. The recordings were performed at 36.0 ± 1.0 °C and we employed the same pacing protocol as for the optical AP recordings. To analyze CMs with the same beating rate, CMs with self-beating faster than 1 Hz were excluded from the analysis. The fluorescent images with Fluo-8 was analyzed by averaging the pixel intensities in the regions of interest drawn to include the whole cell. To eliminate the differentials in observed fluorescence intensities affected by Fluo-8 loading efficiency and cell lines, loading and acquisition conditions were kept as consistent as possible, and all absolute fluorescence values (F) were normalized to fluorescence value at resting (F_0) and presented as $\Delta F/F_0 = (F-F_0)/F_0$. Abnormal Ca^{2+} waves were defined as non-stimulated increases (at least 3% of the Ca^{2+} transient amplitude) in the intracellular Ca^{2+} levels. A solution containing 100 nM isoproterenol was prepared immediately before the experiment, applied to the cells for 5 min, and the recordings were performed in the same way as the baseline condition.

3. Assessment of Ca^{2+} homeostasis

Ca^{2+} storage capacity of the sarcoplasmic reticulum (SR Ca^{2+} load) and RyR2-mediated SR Ca^{2+} leakage (SR Ca^{2+} leak) were assayed using Fluo-8 fluorescence and the Shannon-Bers technique.[30] The single isolated iPSC-CMs (5-6 weeks old) were loaded in the same way as the Ca^{2+} transient recording described above. The recordings were performed at 36.0 ± 1.0 °C. Cells were bathed in NT solution and field-stimulated at 1 Hz (20-30 V, 4 ms) for at least 20 secs to bring the intracellular Ca^{2+} content to a steady state. Then stimulation was turned off, and the bath solution was rapidly switched to a Na^+/Ca^{2+}-free buffer containing (in mmol/L): 140 LiCl, 5.4 KCl, 0.53 $MgCl_2$, 5 HEPES, 10 glucose, 10 EGTA, and with LiOH to adjust the pH to 7.4, for approximately 30 secs to completely abolish Ca^{2+} fluxes through the Na^+/Ca^{2+} exchanger and reach a stable condition. Then the bath solution was rapidly switched to a 1 mM tetracaine (0 Na^+, 0 Ca^{2+}) solution for approximately 20 secs to completely inhibit the RyR2 channels. Finally, SR Ca^{2+} stores were depleted by rapidly switching the bath solution to a 30 mM caffeine (0 Na^+, 0 Ca^{2+}) solution for approximately 20 secs. Fluo-8 fluorescence was recorded from the last 5 secs of the 1 Hz pacing to the end of caffeine solution perfusion. The temperature of the reflux solution was controlled using a handmade water jacket system and was quickly switched using a Micromanifold (100 μm ID Tip; World Precision Instruments, Sarasota, FL, USA). Absolute fluorescence values were normalized as in the Ca^{2+} transient recording described above. $F_{diastole}$ and F_{leak} were separately defined as the average level of the last 3 secs of the Na^+/Ca^{2+}-free buffer or tetracaine solution bathing. $F_{caffeine}$ was defined as the maximum value after switching to the caffeine solution. To eliminate differences among cell lines and recordings, SR Ca^{2+} leak and SR Ca^{2+} load were calculated with the equations below.

$$\text{SR } Ca^{2+} \text{ leak} = (F_{diastole} - F_{leak})/F_{diastole}$$
$$\text{SR } Ca^{2+} \text{ load} = (F_{caffeine} - F_{leak})/F_{leak}$$

Whole-cell patch-clamp recordings in iPSC-CMs

For patch-clamp recordings, the iPSC-CMs (5-6 weeks old) were dispersed with collagenase B and Trypsin EDTA into single cells and plated onto glass coverslips. The isolated single cells were maintained additional 3-5 days in the medium containing DMEM/F12 with 2% FBS before recordings.

1. AP recording using a whole-cell patch clamp technique

AP waveforms were recorded using a ruptured whole-cell patch-clamp technique at 36 ± 1℃. Data were acquired at 10 kHz using the Multiclamp 700B amplifier, Digidata 1440 digitizer hardware, and pClamp 10.4 software (Molecular Devices, Sunnyvale, CA, USA). AP waveforms were recorded during spontaneous beating and under 1 Hz pacing. The patch glass pipette tip resistance was between 3 to 5 MΩ. The bath solution is comprised of (mmol/L): 150.0 NaCl, 5.4 KCl, 1.8 $CaCl_2$, 1.0 $MgCl_2$, 15.0 glucose, 15.0 HEPES, and 1.0 Na-pyruvate with pH of 7.4. The pipette solution is comprised of (mmol/L): 150.0 KCl, 5.0 EGTA, 5.0 MgATP, 10.0 HEPES, 5.0 NaCl, 2.0 $CaCl_2$ with pH of 7.2, and 300 μg/ml amphotericin B. The ventricular-like iPSC-CMs were distinguished by the presence of a marked plateau phase resulting in a longer APD and an APD_{90}/APD_{50} ratio in the range of 1.1 to 1.3.[18, 29]

2. L-type Ca^{2+} channel (LTCC) current recording

LTCC currents were recorded using a ruptured whole-cell patch-clamp technique at room temperature[8, 18] using the same equipment as AP recording. Bath solution was comprised of (mmol/L): 140.0 TEA-Cl, 5.4 CsCl, 1.8 $CaCl_2$, 1.2 $MgCl_2$-$6H_2O$, 5.0

HEPES, 10.0 Glucose, 1.0 4-aminoprydine, and with CsOH to adjusted pH to 7.4. The pipette solution was comprised of (mmol/L): 20.0 TEA-Cl, 120.0 CsCl, 3.0 $MgCl_2$-$6H_2O$, 10.0 EGTA, 5.0 MgATP, and 5.0 HEPES. Pipettes had tip resistances between 2-3 MΩ. The parameters of the voltage dependent activation and inactivation were obtained by fitting with the Boltzmann equation: $I/I_{max} = 1/[1 + \exp(V-V_{1/2})/k]$, where $V_{1/2}$ is the voltage at which LTCC currents are half-maximally activated and k is the slope factor. Currents between −10 and +10 mV were fitted with a single exponential function to obtain inactivation time constants.

Generation of inducible HEK293 cell lines stably expressing RyR2

Full-length mouse RyR2 cDNA was PCR-amplified from mouse ventricles and cloned into a tetracycline-induced expression vector (pcDNA5/FRT/TO; Life Technologies, CA, USA).[19] The expression vector was transfected with Flp-In T-Rex HEK293 cells (Life Technologies).[19] Clones with suitable doxycycline-induced expression of RyR2 were selected and used for experiments.

Imaging of Ca^{2+} dynamic in the cytosol and endoplasmic reticulum (ER) in HEK293 cells expressing RyR2 channels

RyR2-HEK293 cells cultured in a glass-bottom dish were transfected with calmodulin-IRES-CFP Baculovirus (expressing WT-, E46K- or N98S-CaM) and induced with doxycycline at the same time. Single cell Ca^{2+} imaging of HEK293 cells was performed 20-24 hours after induction with doxycycline. For cytoplasmic Ca^{2+} monitoring, cells were loaded with Fluo-4 AM (Life Technologies) for 30 min at 37˚C and then incubated with normal Krebs solution (140 mM NaCl, 5 mM KCl, 2 mM $CaCl_2$, 1 mM $MgCl_2$, 11 mM glucose, and 5 mM HEPES; adjusted pH to 7.4). Fluo-4 was excited at 488 nm, and fluorescence signals at wavelengths longer than 525 nm were acquired using an

inverted microscope (TE2000E, Nikon) equipped with an EM-CCD camera and AquaCosmos software (Hamamatsu Photonics, Hamamatsu, Japan). Ca^{2+} signals were obtained in normal Krebs solution for 5 min and then in caffeine containing Krebs solution. At the end of each measurement, cells were treated with a 20Ca-Krebs solution containing 20 μM ionomycin (#19068-31; Calbiochem/Merck, Darmstadt, Germany) and 20 mM $CaCl_2$ to obtain F_{max} of Fluo-4. Fluorescence signals in individual cells were determined using region of interest (ROI) analysis and expressed as F/F_{max}.

ER luminal Ca^{2+} signals were obtained using a genetically encoded Ca^{2+} indicator R-CEPIA1er[20] (a gift from Dr Masamitsu Iino, The University of Tokyo, K_D = 565 nM, n = 1.71) using the same imaging system as described above. Fluorescent Ca^{2+} signals were measured in the normal Krebs solution and then in the Krebs solution containing caffeine. At the end of each measurement, F_{min} and F_{max} of the Ca^{2+} indicator were obtained with a Ca^{2+}-free Krebs solution containing 20 μM ionomycin, 5 mM BAPTA, and 20 μM cyclopiazonic acid and a 20Ca-Krebs solution. Fluorescence Ca^{2+} signals in individual cells were expressed as $(F-F_{min})/(F_{max}-F_{min})$.

[^{3}H]Ryanodine binding assay

[^{3}H]Ryanodine binding was performed on HEK293 cell microsomes.[21] Microsomes (50–100 μg of protein) were incubated with 5 nM [^{3}H]ryanodine for 1 h at 25°C in the binding buffer (0.17 M NaCl, 20 mM MOPSO, pH 7.0, 2 mM dithiothreitol, 1 mM $MgCl_2$, 1 mM AMP) containing various concentrations of free [Ca^{2+}] and WT-/N98S-/E46K-CaM. The protein-bound [^{3}H]ryanodine was separated by filtering through polyethyleneimine-treated glass filters (Whatman GF/B; Whatman, Maidstone, UK). Nonspecific binding was determined in the presence of 20 μM unlabeled ryanodine. The [^{3}H]ryanodine binding data were normalized to the maximal binding for

[^{3}H]ryanodine (B_{max}), which was separately determined by Scatchard plot analysis using varied concentrations of [^{3}H]ryanodine (3–20 nM) in the medium containing 1 M NaCl. The resultant B/B_{max} represents an averaged activity of individual channels and thereby compares quantitatively the effect between WT and mutated CaMs.

Measurement of CaM-Ca^{2+} binding affinity

Recombinant CaM proteins (WT-, E46K-, or N98S-CaM) were expressed in E. coli and purified using the previously established method.[19] The macroscopic binding constants for Ca^{2+} binding to CaMs were determined as described previously.[22] Binding to CaM N-domain was monitored by phenylalanine fluorescence using excitation at 250 nm and emission at 280 nm. Binding of Ca^{2+} to CaM C-domain was monitored by tyrosine fluorescence using excitation at 277 nm and emission at 320 nm. The free [Ca^{2+}] level at each point during the course of a Ca^{2+} titration was determined by the extent of saturation of a Ca^{2+} indicator dye, Oregon Green 488 BAPTA-5N (0.1 μM; Invitrogen, Carlsbad, CA, USA) as the equation:

$$[\mathrm{Ca}^{2+}]_{free} = K_D \frac{f_{[high]} - f_{[X]}}{f_{[X]} - f_{[low]}}$$

The normalized fluorescence signals were plotted as a function of free [Ca^{2+}] levels, and the data were fitted to the model-independent 2-site Adair function as described previously.[22] The dissociation constants (K_D) for each domain were reported as average values for the pair of sites by taking the square root of K_2 from the Adair equation. All titrations were repeated three times.

Bio-Layer Interferometry (BLI)-based CaM-RyR2 binding assay

The BLI analyses were performed using the Octet RED 96 system (ForteBio, CA, USA) in order to measure the binding affinity between CaM (WT/E46K/N98S) and His-

FKBP12.6-RyR2 at low or high [Ca^{2+}] levels. Ni-NTA biosensors (Fortebio) were prewetted with the ligand buffer (500 mM NaCl, 20 mM MOPS-N, 0.015% Tween-20, and 2 mM DTT; adjusted pH to 7.4) for 10 min before the assay. The assay was performed in 96-well plates at a volume of 200 μL per well while shaking the plates at 1000 rpm at 25 °C. For the initial step, the biosensors were kept with the ligand buffer for 60 secs. The biosensors were then loaded with the His-FKBP12.6-RyR2 sample (0.12 mg/ml) in the ligand buffer for 1800 secs. Then, the loaded biosensors were washed for another 300 secs in low or high Ca^{2+} assay buffers (150 mM NaCl, 20 mM MOPS-N, 0.015% Tween-20, 2 mM DTT, and 30 nM or 100 μM $CaCl_2$; adjusted pH to 7.4). Subsequently, the biosensors were moved into corresponding assay buffers, containing CaMs with varying concentrations, in a series of 3-fold dilutions for 300 secs. Finally, the biosensors were moved into an assay buffer without CaMs for 300 secs. The data were processed and analyzed using the Octet Data Analysis Software (Fortebio). The response profiles were globally fitted using a 1:1 complex model after baseline subtractions with the signal of a reference biosensor (run with a no CaM buffer). And kinetic parameters such as the association (k_{on}) and the dissociation (k_{off}) rates, and the binding affinity constants ($K_D = k_{off}/k_{on}$) were calculated and obtained by the software. The k_{on}, k_{off}, and K_D were compared among WT and mutated CaMs. A smaller K_D value indicates a higher binding affinity ($1/K_D$).

Drug testing in *CALM2* p.E46K iPSC-CMs

CALM2 p.E46K iPSC-CMs were used for drug testing. A series of four consecutive Ca^{2+} transient recordings was performed at baseline and applied with 1, 3, and 10 μM nadolol or flecainide (Sigma-Aldrich). Frequency of abnormal Ca^{2+} waves and Ca^{2+} transient amplitudes were calculated and used to evaluate the antiarrhythmic effect.

Supplemental Tables

Supplemental Table I

Targeted 60 genes for target exon sequencing

AKAP9	*CTNNA3*	*KCNE1*	*KCNQ1*	*SCN2B*
ANK2	*DPP6*	*KCNE2*	*LMNA*	*SCN3B*
CACNA1C	*DSC2*	*KCNE3*	*MYBPC3*	*SCN4B*
CACNA2D1	*DSG2*	*KCNE4*	*MYH6*	*SCN5A*
CACNB2	*DSP*	*KCNE5*	*NCS1*	*SLC8A1*
CALM1	*GJA1*	*KCNH2*	*NKX2-5*	*SNTA1*
CALM2	*GJA5*	*KCNIP2*	*PKP2*	*TBX5*
CALM3	*GPD1L*	*KCNJ2*	*PRKAG2*	*TCAP*
CAMK2D	*HCN4*	*KCNJ3*	*RANGRF*	*TECRL*
CASQ2	*JUP*	*KCNJ5*	*RYR2*	*TMEM43*
CAV3	*KCNA5*	*KCNJ8*	*SCN10A*	*TRDN*
CHRM2	*KCND3*	*KCNN2*	*SCN1B*	*TRPM4*

Supplemental Table II

Custom oligonucleotides for primers and gene editing

Gene	Experiment	Sequence	
CALM1	qPCR	Forward	AGGGAGAAGGCTTCCTTGAA
		Reverse	CTCGCTCCCTCTGCTCTTC
CALM2	qPCR	Forward	CTCGTTTGCGATGTTCCGTTAT
		Reverse	AGCGCCTCATAAACACCTCC
CALM3	qPCR	Forward	CCGGGCAATATTGTGTTCAGTT
		Reverse	GAGGAGCCAAATCAGGTAGT
RYR2	qPCR	Forward	CAAATCCTTCTGCTGCCAAG
		Reverse	CGAAGACGAGATCCAGTTCC
CACN1C	qPCR	Forward	CGGGCATGCTTGATCAGAAG
		Reverse	CCGCAGTTTTCTCCCTCGAT
ATP2A2	qPCR	Forward	TCAGCAGGAACTTTGTCACC
		Reverse	GGGCAAAGTGTATCGACAGG
SLC8A1	qPCR	Forward	CTGGAATTCGAGCTCTCCAC
		Reverse	ACATCTGGAGCTCGAGGAAA
CASQ2	qPCR	Forward	TTATGTTCAAGGACCTGGGC
		Reverse	GCCTCTACTACCATGAGCCG
SCN5A	qPCR	Forward	TGCTGTGAAAATCCCTGTGA
		Reverse	TCAACACACTCTTCATGGCG
KCNQ1	qPCR	Forward	CGCCTGAACCGAGTAGAAGA
		Reverse	TGAAGCATGTCGGTGATGA
GAPDH	qPCR	Forward	CTGGGCTACACTGAGCACC
		Reverse	AAGTGGTCGTTGAGGGCAATG
CALM2 exon 3	Gene editing	crRNA	TCCTGTAACTCTGCTTTTGTGGG
CALM2 exon 3	Gene editing	ssODN	ATTGGGAACTGTAATGAGATCTCTTGGGCAGAATCCCACAG AAGCAGAGTTACAGGACATGATTAATGAAGTAGATGCTGA
CALM2 exon 3-5	PCR	Forward	ACGATCCCACCACTGAGTAG
		Reverse	CCTTCCTTTCCCACCTTCAC
CALM2 exon 3-5	On target Sequencing	Seq 1	TAGATGCTGATGGTAAGTC
		Seq 2	TGTATTGCGTTCATCTTGTC
		Seq 3	GGTGATGGTCAAGTAAACTATG
		Seq 4	ATAGGATTCTTGGGTGATTC
		Seq 5	CTGGGCAATAAACTAGCTTC
		Seq 6	TCTAAGCCCTTCTGCACATC
-	Off target #1 sequencing	Forward	TTACGGATGGCAGGTCCTTG
		Reverse	AGACTGGACTTCAGGGTTTG
	Off target #2 sequencing	Forward	GGCACTTGGCTTGTAACAAC
		Reverse	GTTGCTTCTGCTACCATCTG
	Off target #3 sequencing	Forward	AATCATTCCAGGTGCCCATC
		Reverse	TGAGTTCTCCTGCCTCTTTC

qPCR: quantitative polymerase chain reaction; crRNA: CRISPR RNA;
ssODN: single-stranded oligodeoxynucleotide; Seq: sequencing

Supplemental Table III

Other rare variants except for *CALM2* p.E46K identified in the probands by target sequencing of 60 genes

Patient	Gene	Ref. ID	Nucleotide	Amino Acid	dbSNP	ACMG classification
Proband 1	*DSG2*	NM_001943.4	1597G>A	V533I	rs199761749	Benign (BS1, BS2, BP4)
Proband 2	*CACNA1C*	NM_000719.7	5609C>T	T1870M	rs201777030	Benign (BP6, BS1, BS2, BP4)
Proband 2	*PKP2*	NM_004572.4	243G>A	D812N	rs200947767	Benign (BS1, BS2, BP4)
Proband 2	*TRPM4*	NM_017636.4	3098T>A	I1033N	-	Uncertain Significance (PM5, PM2)

Ref.: Reference sequence; ACMG: American College of Medical Genetics; BS: Strong evidence of benign impact; BP: Supporting evidence of benign impact; PM: Moderate evidence of pathogenicity.

Supplemental Table IV

Potential off-target sites in CRISPR-Cas9 gene editing

No.	Sequence	Chr	Strand	Position	Number of mismatches
#1	GCC--TATCTCTGCTTTTGT	3	+	115372544	4
#2	ACCTGTTTCTCTGCTTTTGT	18	+	51942008	3
#3	TTTTGTAACTCTACTTTTGT	X	-	125551554	3

Chr: chromosome; Red characters indicate the mismatches in the gRNA compared to the off-target sites. The off-target sites were predicted by CRISPR-Cas9 guide RNA design checker (https://sg.idtdna.com/site/order/designtool/index/CRISPR_SEQUENCE).

Supplemental Table V

Characteristics of action potential parameters obtained by patch-clamp recordings

	Spontaneous Beating			1 Hz Pacing		
Parameters	Ctr (*n* = 14)	E46K (*n* = 16)	E46K-Cor (*n* = 16)	Ctr (*n* = 10)	E46K (*n*= 8)	E46K-Cor (*n* = 8)
APA (mV)	107.2 ± 2.3	105.9 ± 3.3	104.8 ± 3.8	103.2 ± 3.1	102.8 ± 2.6	105.1 ± 2.2
MDP (mV)	-68.6 ± 5.5	-70.2 ± 5.5	-65.8 ± 5.4	-70.8 ± 3.2	-71.2 ± 6.2	-70.6 ± 4.8
APD_{90} (ms)	247.6 ± 28.3	261.6 ± 33.9	265.7 ± 24.1	201.6 ± 14.2	203.3 ± 11.3	206.2 ± 10.3
APD_{50} (ms)	203.0 ± 23.2	204.4 ± 26.5	209.2 ± 19.0	166.4 ± 10.2	167.1 ± 9.6	165.7 ± 12.2

Ctr: control; E46K-Cor: *CALM2*-E46K-Corrected isogenic control; Spon.: spontaneous beating; APA: action potential amplitude; MDP: maximum diastolic potential; APD_{90} and APD_{50}: action potential duration at 90% and 50% repolarization, respectively. Statistical analyses were performed using one-way analysis of variance followed by post hoc Tukey's tests. Data are presented as mean ± SEM.

Supplemental Table VI

Clinical characteristics of CPVT-related CaM variants

CaM variant	*CALM1*-N54I	*CALM1*-N98S	*CALM2*-N98S	*CALM3*-A103V	*CALM2*-E46K
Associated arrhythmias	CPVT, SUD	LQTS, CPVT	LQTS, CPVT, SUD, IVF	CPVT	CPVT
No. of families (CPVT / total)	1/2	1/5	1/5	1/1	2/2
No. of patients (CPVT / total)	13/14	1/5	1/5	1/1	2/2
***De novo* variant**	No	Yes	Yes	No	Yes
In patients with CPVT					
No. of families / patients	1/13	1/1	1/1	1/1	2/2
Clinical phenotypes (symptomatic / total)	Syncope (13/13), Cardiac arrest (1/13), SCD (2/13), ECG: PVCs, pVT, VF	Cardiac arrest, ECG: PVC, bVT	SCD, ECG: pVT	Syncope, ECG: PVCs, non-sustained VT	Syncope (2/2), Cardiac arrest (1/2), ECG: bradycardia, prominent T wave, bVT, pVT
Treatment	β blocker	β blocker, ICD	(-)	β blocker	β blocker, Flecainide
Prenatal symptom	(-)	(-)	(-)	(-)	Severe sinus bradycardia in utero (1/2)
Structural heart disease	(-)	(-)	(-)	(-)	PDA (2/2)
Extracardiac phenotype	(-)	(-)	(-)	(-)	Neurodevelopmental disorders (2/2)
Reference	(7)	(7)	(26)	(11)	**This study**

CPVT: catecholaminergic polymorphic ventricular tachycardia; CaM: calmodulin; SUD: sudden unexpected death; LQTS: long QT syndromes; IVF: idiopathic ventricular fibrillation; SCD: sudden cardiac death; ECG: electrocardiogram; PVC: premature ventricular contraction; bVT/pVT: bidirectional/polymorphic ventricular tachycardia; VF: ventricular fibrillation; ICD: implantable cardioverter defibrillator; PDA: patent ductus arteriosus

Supplemental Table VII

Functional characteristics of CPVT-related mutated CaMs

Mutated CaM		**N54I**	**A103V**	**N98S**			**E46K**	
Experimental system		HEK293 cell/ permeabilized mice CM expressing mutated CaM	Same as left	Same as left	HEK293 cell expressing mutated CaM	Patient-derived iPSC-CM	HEK293 cell expressing mutated CaM	Patient-derived iPSC-CM
Electro physiological features		Spontaneous Ca^{2+} wave frequency ↑	Same as left	Same as left	Spontaneous Ca^{2+} wave frequency ↑ $[Ca^{2+}]_{ER}$: threshold ↓, nadir ↓	Prolonged APD_{90} No EAD/DAD Abnormal Ca^{2+} waves↑, SR Ca^{2+}: leak ↑, load ↓	Spontaneous Ca^{2+} wave frequency ↑↑* $[Ca^{2+}]_{ER}$: threshold ↓↓*, nadir ↓	Normal APD_{90} EAD/DAD ↑↑* Abnormal Ca^{2+} wave ↑↑*, SR Ca^{2+}: leak ↑↑*, load ↓↓*
Ca^{2+} affinity		Normal	Decreased in C-domain	Decreased in C-domain	Decreased in C-domain		Normal	
Effect on LTCC		Not changed	Mildly impaired CDI	Impaired CDI	Impaired CDI in iPSC-CM (8)		Not changed in iPSC-CM	
Effect on RyR2	**Activity**	Open probability ↑	Not examined	Open probability ↑	Channel activity ↑		Channel activity ↑↑*	
	Binding affinity	• low $[Ca^{2+}]^{\dagger}$: 2-fold ↑ than WT • high $[Ca^{2+}]^{\ddagger}$: →	• low $[Ca^{2+}]^{\dagger}$: → • high $[Ca^{2+}]^{\ddagger}$: →	• low $[Ca^{2+}]^{\dagger}$: 2-fold ↑ than WT • high $[Ca^{2+}]^{\ddagger}$: →	• low $[Ca^{2+}]^{\dagger}$: 2-fold ↑ than WT (k_{on} ↑, k_{off} →) • high $[Ca^{2+}]^{\S}$: → (k_{on} →, k_{off} →)		• low $[Ca^{2+}]^{\dagger}$:**10-fold** ↑ than WT (k_{on} ↑↑*, k_{off} ↑) • high $[Ca^{2+}]^{\S}$: **2-fold** ↑ than WT (k_{on} →, k_{off} ↓)	
Reference		(10)	(11)	(10)	**This study**		**This study**	

*: E46K vs. N98S in this study, †: 30 nM $[Ca^{2+}]$, ‡: 30 μM $[Ca^{2+}]$, §: 100 μM $[Ca^{2+}]$, CaM: calmodulin; iPSC: induced pluripotent stem cell; CM: cardiomyocyte; EAD/DAD: early/delayed afterdepolarization; APD_{90}: action potential duration at 90% repolarization; ER: endoplasmic reticulum; SR: sarcoplasmic reticulum; LTCC: L-type calcium channel; CDI: calcium dependent inactivation; k_{on}: association rate; k_{off}: dissociation rate

Supplemental Figures

Supplemental Figure I

ECG during exercise test of the index CPVT patient

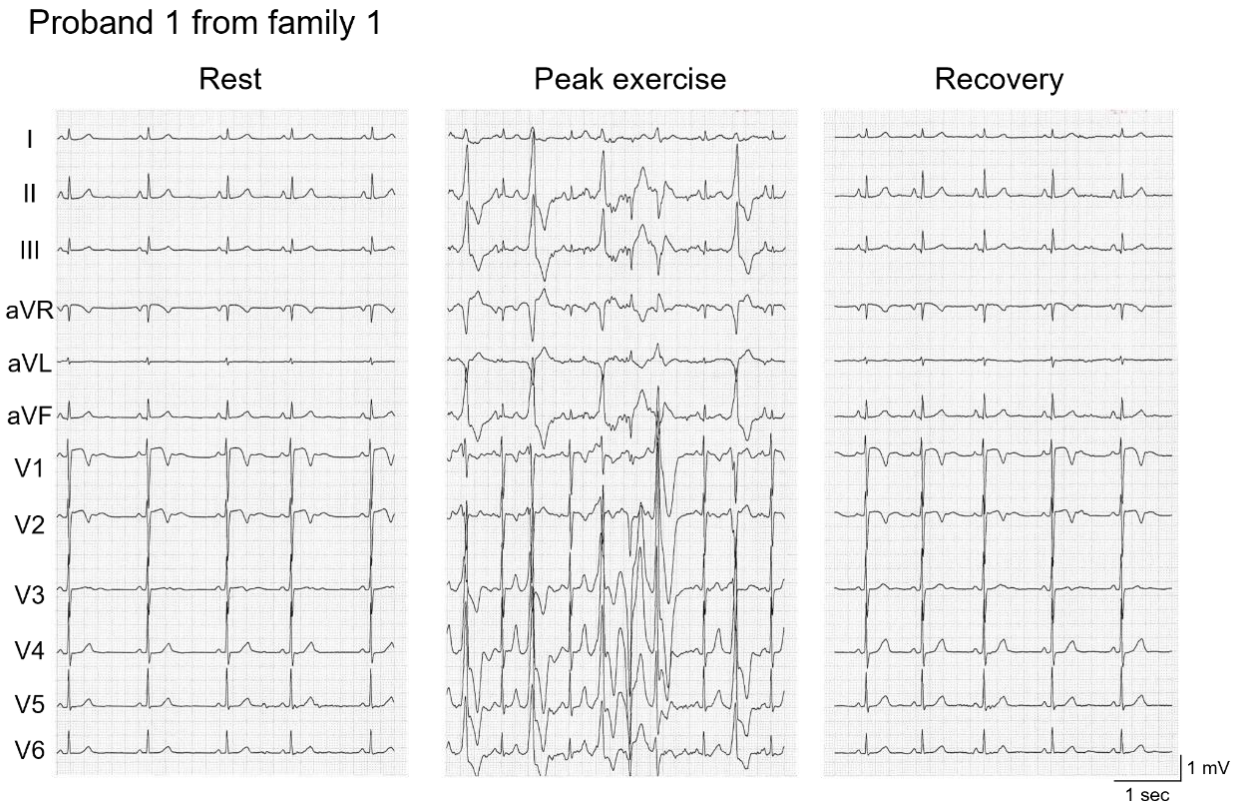

Electrocardiograms (ECGs) during the exercise test of the proband 1 from family 1 at rest (left), peak exercise (middle), and recovery 4 min (right). Polymorphic ventricular tachycardias were observed during exercise (middle).

Supplemental Figure II

Creation of the gene-corrected isogenic control cell line of *CALM2*-E46K

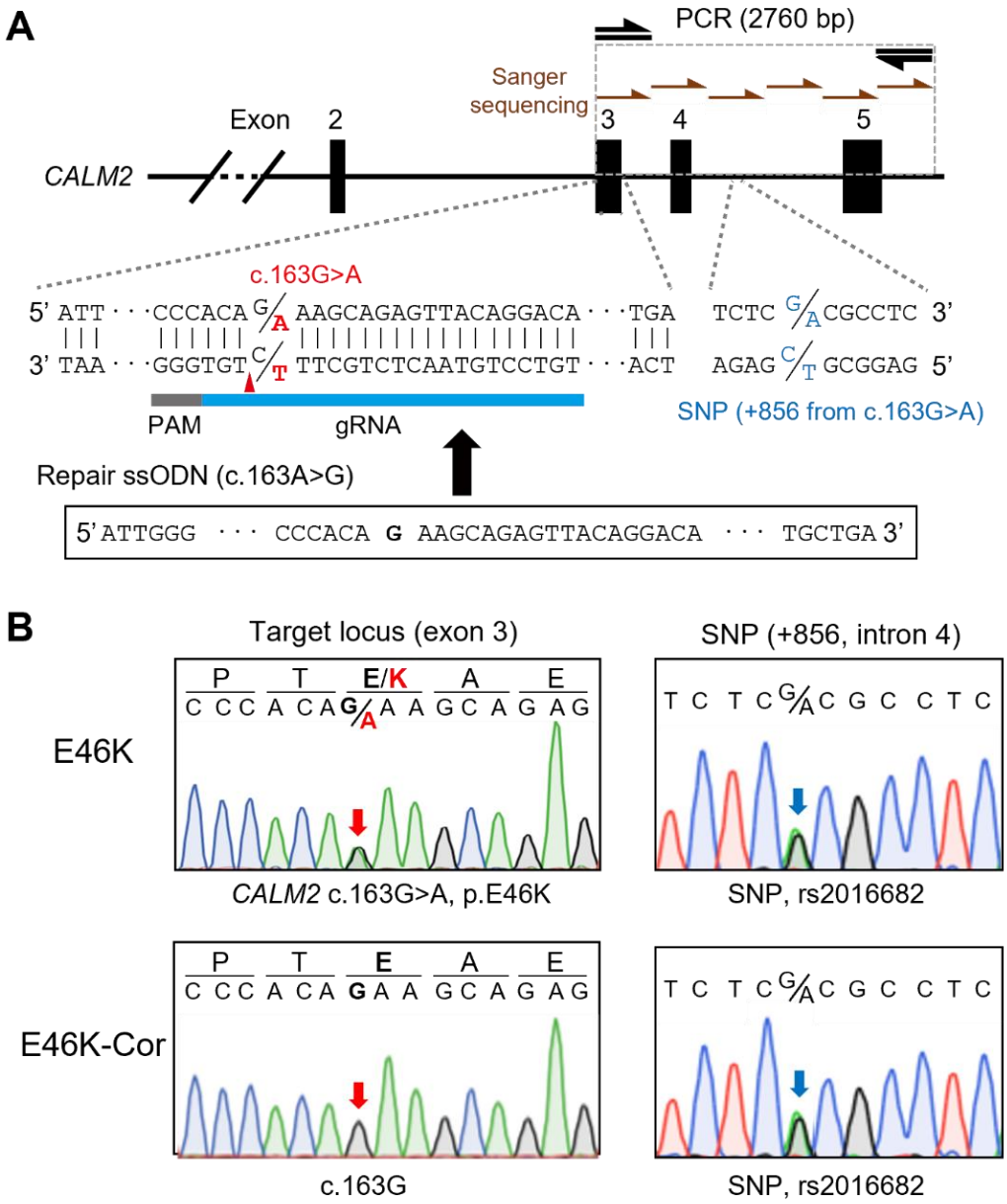

(A) Strategy of the gene correction. Design of a guide RNA (gRNA) is indicated with a blue bar including a protospacer adjacent motif (PAM) site (a gray bar). The variant, c.163 G>A, is indicated in red text. The estimated cut site is indicated with a red triangle. A repair single-stranded oligodeoxynucleotide (ssODN) was used as a donor template. Sanger sequencing of the 2760 bp PCR fragment revealed a heterozygous single nucleotide polymorphism (SNP, blue text) located at 856 bp downstream from the variant site (c.163 G>A). (**B**) Sanger sequences of the *CALM2*-E46K and *CALM2*-E46K corrected (E46K-Cor) iPSCs. The heterozygous variant, c.163 G>A, p.E46K, in E46K iPSC line was successfully corrected in the E46K-Cor iPSC line as indicated with red arrows. The heterozygous SNP (rs2016682) identified in both E46K and E46K-Cor iPSCs (blue arrows) indicate that there is no large deletion resulting from on-target unintended genome modification.

Supplemental Figure III

Characterization of *CALM2*-E46K and *CALM2*-E46K corrected iPSCs

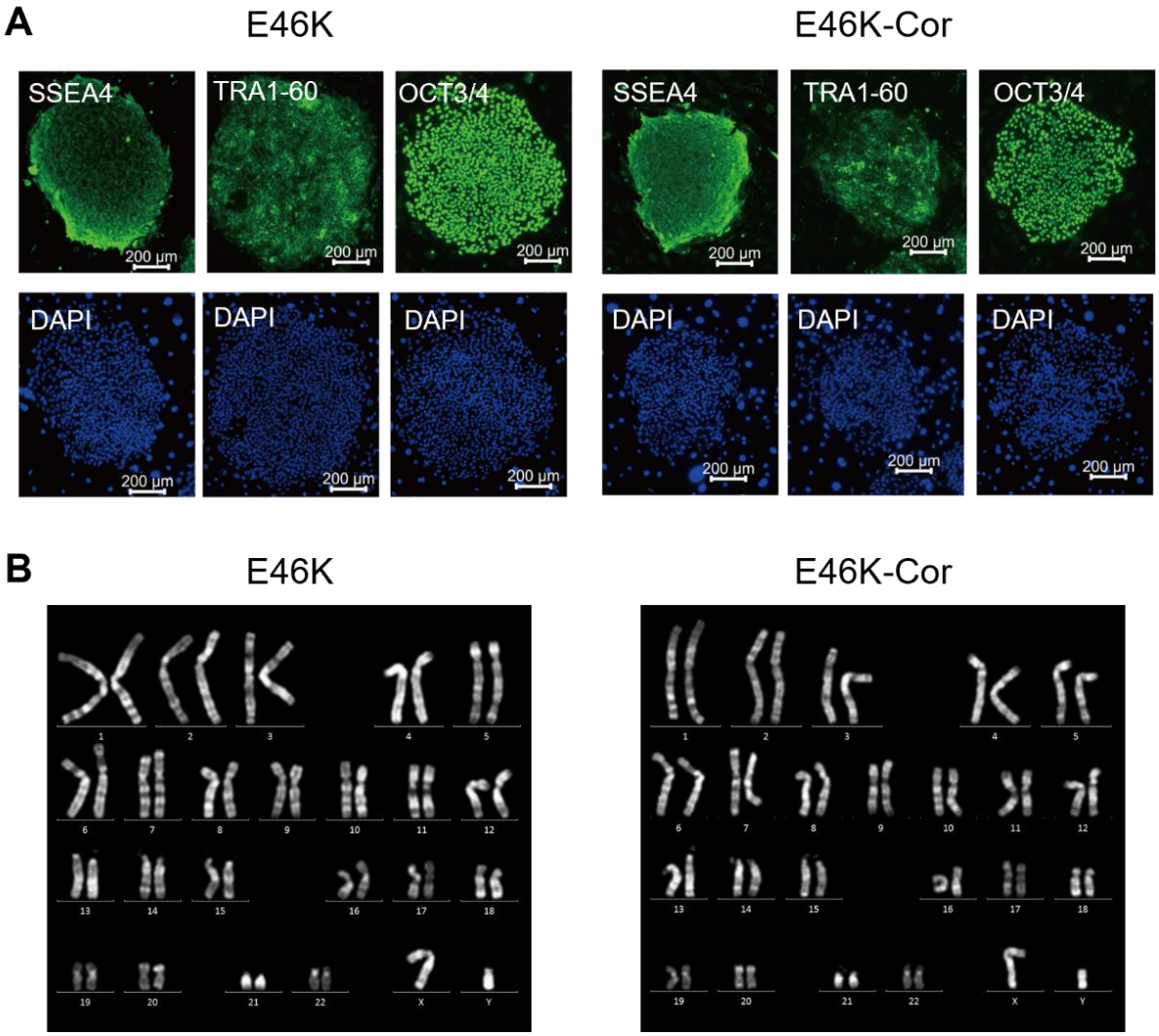

(**A**) Expression of pluripotency markers (SSEA4, TRA1-60, and OCT3/4) in *CALM2*-E46K and *CALM2*-E46K corrected (E46K-Cor) iPSCs. (**B**) The karyotype analysis of iPSCs. Both E46K and E46K-Cor iPSCs maintain a normal karyotype.

Supplemental Figure IV

iPSC cardiac differentiation and characterization of iPSC cardiomyocytes

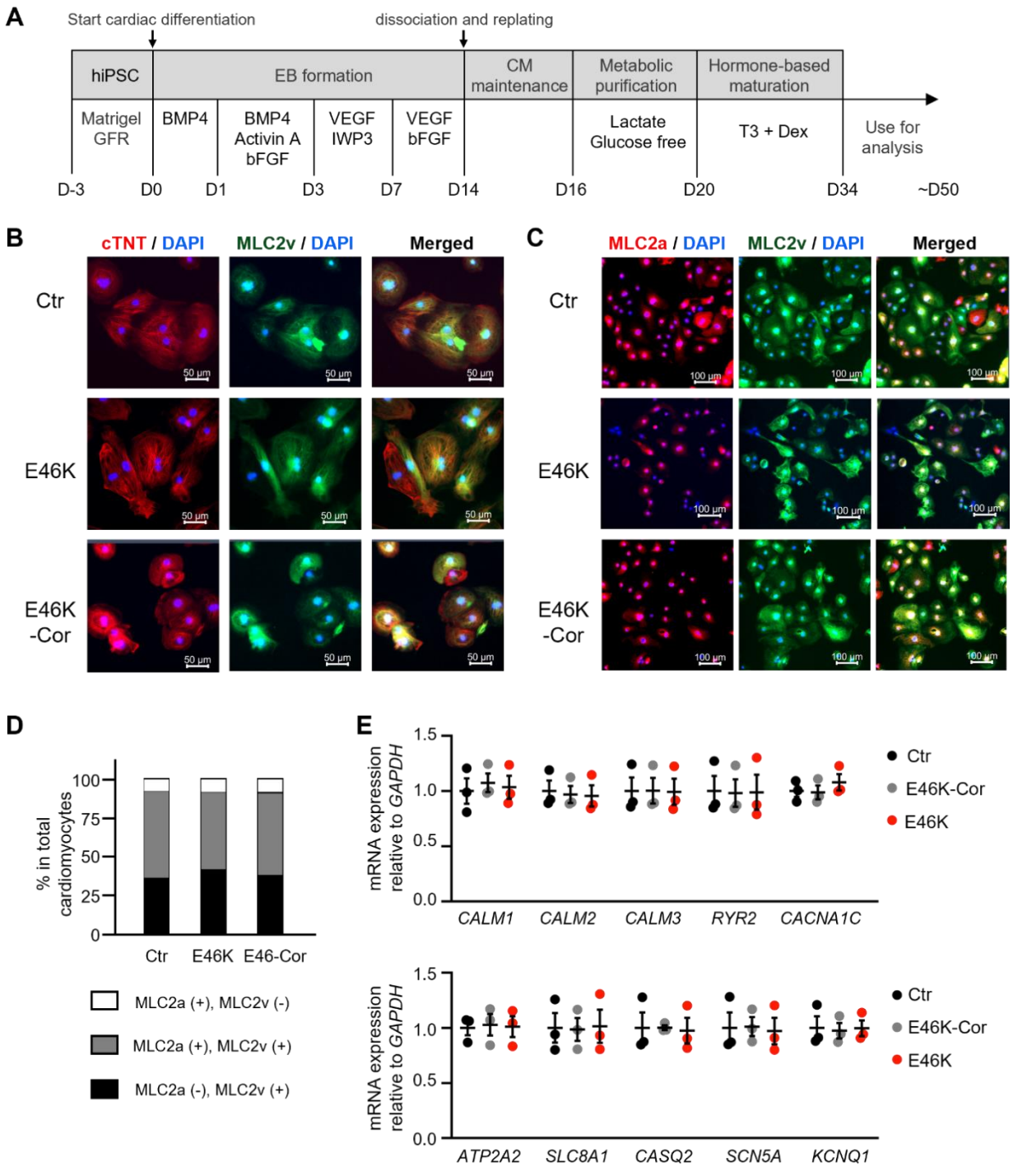

(**A**) Schematic diagram of the iPSC cardiac differentiation protocol. iPSCs were differentiated into cardiomyocytes (CMs) using an embryoid body (EB) differentiating system. The iPSC-CMs were purified in a glucose-depleted lactate medium and further maturated using media supplemented with

triiodo-L-thyronine (T3) and dexamethasone (Dex). The CMs at 5-7 weeks after cardiac differentiation were used for functional analysis. (**B**) Representative immunostaining images of cardiac troponin T (cTnT, red), ventricular-specific myosin light chain 2 (MLC2v, green), DAPI (blue), and merged in iPSC-CMs differentiated from control (Ctr), *CALM2*-E46K, and *CALM2*-E46K-correted isogenic control (E46K-Cor). (**C**) Representative immunostaining images of atrial-specific myosin light chain 2 (MLC2a, red), MLC2v (green), DAPI (blue), and merged in Ctr, E46K, and E46K-Cor iPSC-CMs. (**D**) The percentage of MLC2a or/and MLC2v positive CMs. More than 90% of CMs were MLC2v positive, indicating a high percentage of ventricular-like CMs. (**E**) Relative mRNA expression of the proteins involved in cardiac excitation-contraction coupling were normalized to *GAPDH* in the Ctr (black), E46K-Cor (gray), and E46K (red) iPSC-CMs. Data are shown as means ± SD (n = 3 in each group) and were analyzed by one-way ANOVA and post-hoc Tukey's test. There is no significant difference among three cell lines.

Supplemental Figure V

Action potential durations at 50% repolarization in iPSC-CMs

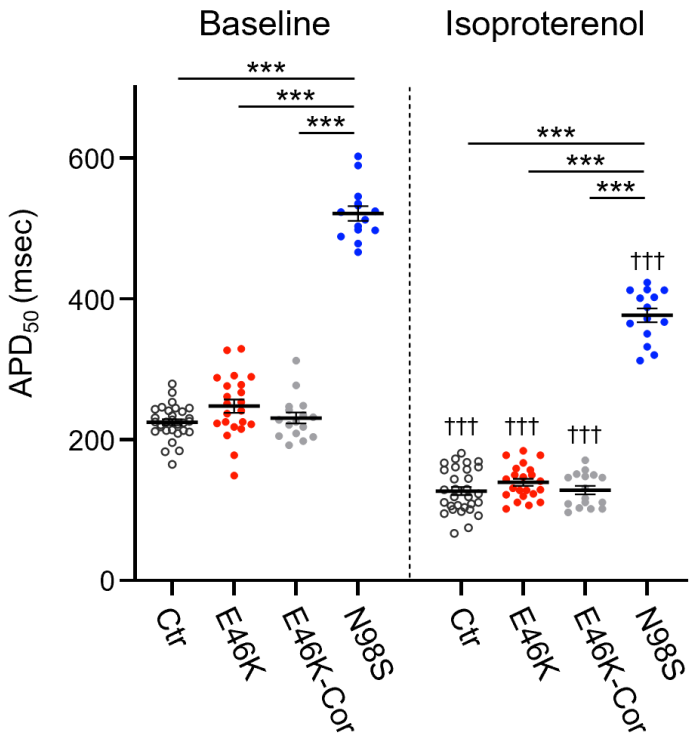

APDs at 50% repolarization (APD_{50}) values recorded using a voltage sensitive dye in control (Ctr), *CALM2*-E46K, *CALM2*-E46K-correted isogenic control (E46K-Cor), and *CALM2*-N98S monolayer iPSC-derived cardiomyocytes (iPSC-CMs) at baseline (left) and after 100 nM isoproterenol treatment (right). Data are from Ctr (n = 32), E46K (n = 22), E46K-Cor (*n* = 16), and N98S (*n* = 14). The data are shown as mean ± SEM. Comparisons between before and after isoproterenol treatment in each cell line were analyzed using two-tailed paired t-test ($^{\dagger\dagger\dagger}p < 0.001$ vs. baseline). Comparisons among multiple cell lines at baseline or after isoproterenol treatment were analyzed by one-way ANOVA and post-hoc Tukey's test (***$p < 0.001$).

Supplemental Figure VI

Conduction velocity (CV) measurements in iPSC-CM sheets

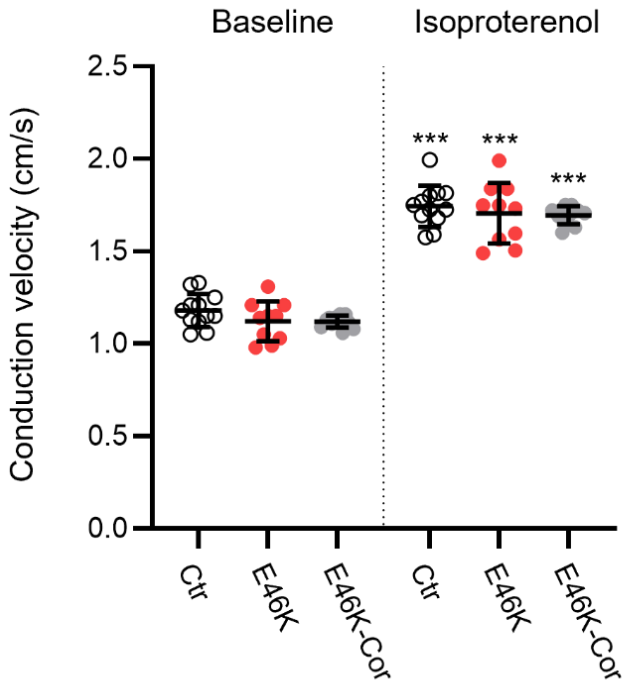

The CV was analyzed by using the action potential map of the iPSC-derived cardiomyocyte (iPSC-CM) sheets recorded using a voltage sensitive dye under 1 Hz pacing at baseline and after isoproterenol treatment. Data are from Ctr (n = 12), E46K (n = 10), and E46K-Cor (*n* = 11). The data are shown as mean ± SEM. Comparisons between before and after isoproterenol treatment in each cell line were analyzed using two-tailed paired t-test (***$p < 0.001$ vs. baseline). Comparisons among multiple cell lines at baseline or after isoproterenol treatment were analyzed by one-way ANOVA and post-hoc Tukey's test.

Supplemental Figure VII

Action potential (AP) recording in iPSC-CMs using a patch-clamp technique

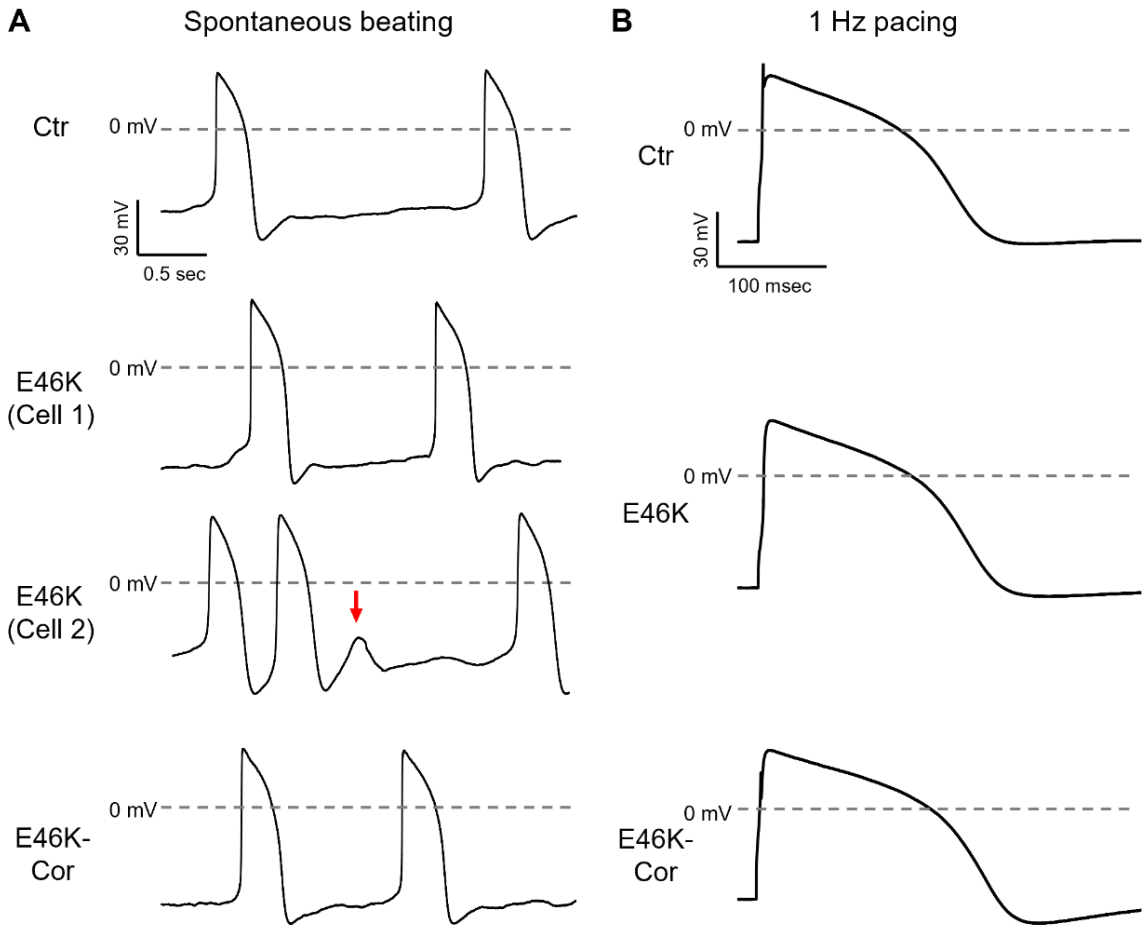

(**A**) Representative AP traces recorded using a whole-cell patch-clamp technique in control (Ctr), *CALM2*-E46K, and *CALM2*-E46K-correted isogenic control (E46K-Cor) isolated iPSC-derived cardiomyocytes (iPSC-CMs) during spontaneous beating. Red arrow indicates an abnormal depolarization. (**B**) Representative AP traces recorded in Ctr, E46K, and E46K-Cor iPSC-CMs under 1 Hz pacing.

Supplemental Figure VIII

Characteristics of abnormal Ca^{2+} waves in iPSC-CMs with CaM variants

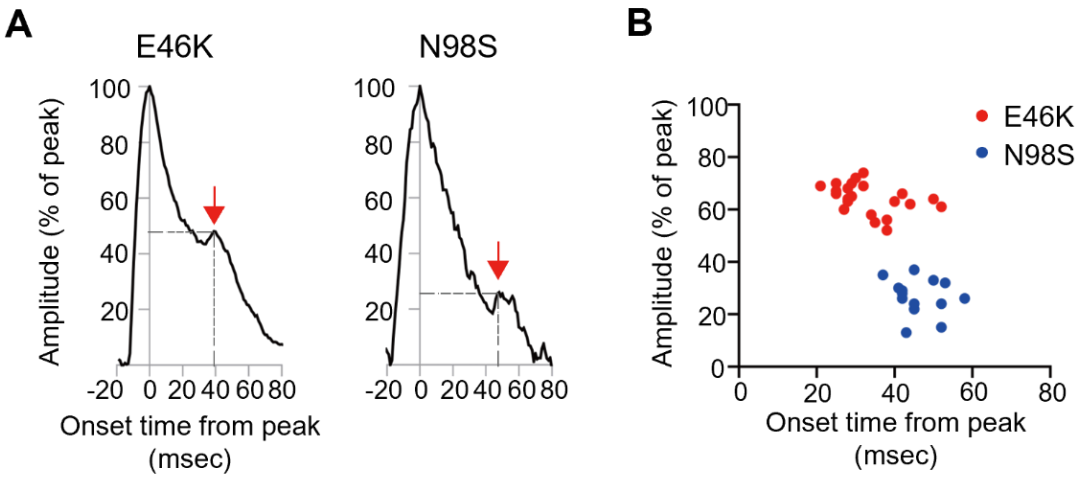

(**A**) Representative traces of abnormal Ca^{2+} waves in Ca^{2+} transient recordings from isolated single *CALM2*-E46K and *CALM2*-N98S iPSC-derived cardiomyocytes (iPSC-CMs). Red arrows indicate the peak point of the abnormal Ca^{2+} waves. Dashed lines indicate the onset time from peak and the amplitude (percentage of peak) of the abnormal Ca^{2+} waves. (**B**) Scatter plot showing the characteristics of the abnormal Ca^{2+} waves in E46K (red, $n = 24$) and N98S (blue, $n = 14$). The two-tailed unpaired t-test showed that the values in both the x-axis and the y-axis were significantly different between E46K and N98S ($p < 0.001$ for both axis).

Supplemental Figure IX

Western blot image of WT and mutated CaMs expressed in RyR2-HEK293 cells

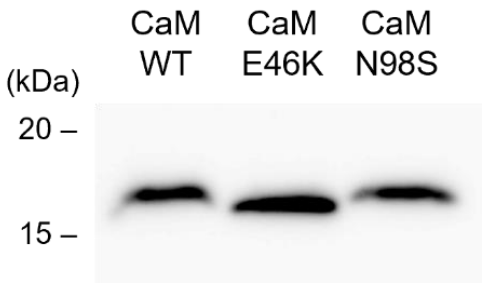

Total cell lysates from RyR2-HEK293 cells infected with WT, E46K, or N98S CaM baculovirus were processed on SDS-PAGE with 15% gel and blotted with anti-CaM antibody. Note that similar amount of CaM was expressed. Mobility for CaM-E46K was slightly faster than those for WT and N98S.

Supplemental Figure X

SDS-PAGE of the purified proteins used for BLI-based CaM-RyR2 binding assay

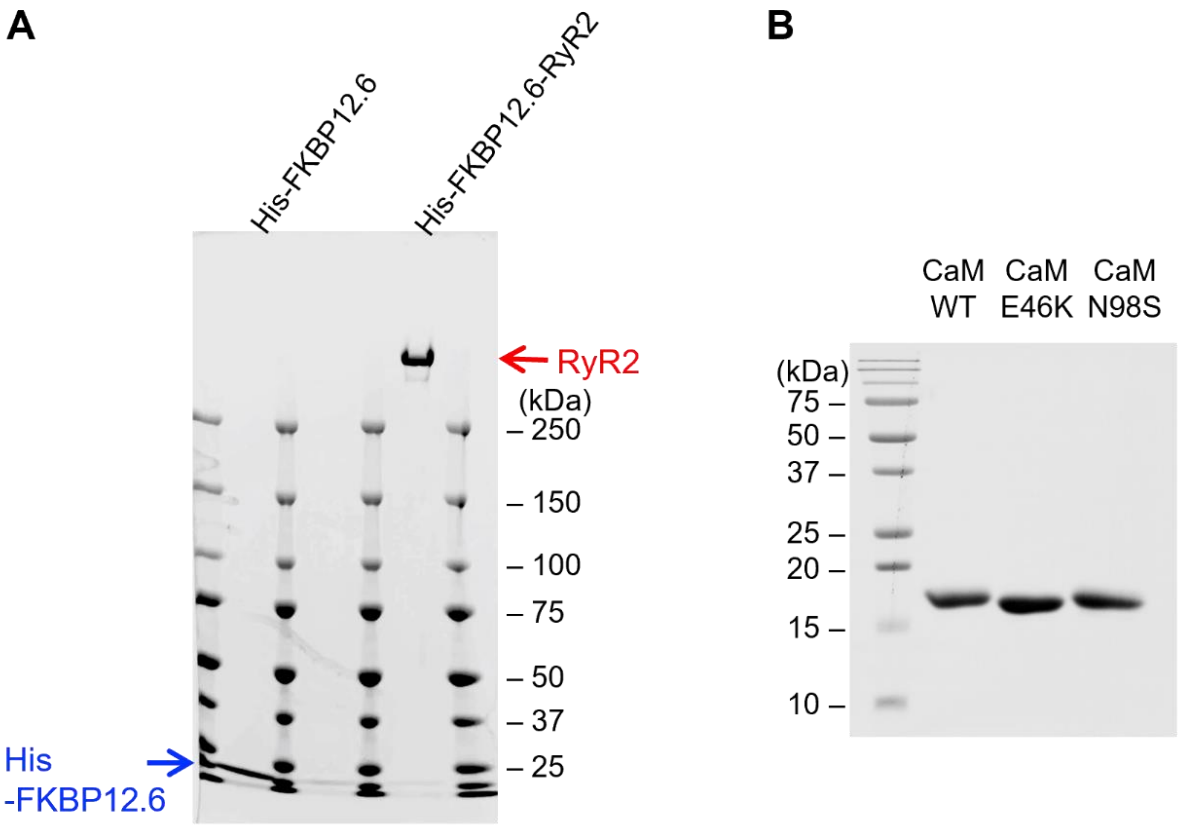

(**A**) His-FKBP12.6 and His-FKBP12.6-RyR2 complex. (**B**) WT and mutated CaMs. Proteins were processed on SDS-PAGE with a 3-15% gradient gel (**A**) or a 15% gel (**B**) and stained with Coomassie Brilliant Blue. Note that mobility for CaM-E46K was slightly faster than those for WT and N98S. BLI: bio-layer interferometry.

Supplemental Figure XI

Representative real-time CaM-RyR2 binding traces obtained by the biolayer interferometry (BLI)-based Octet system

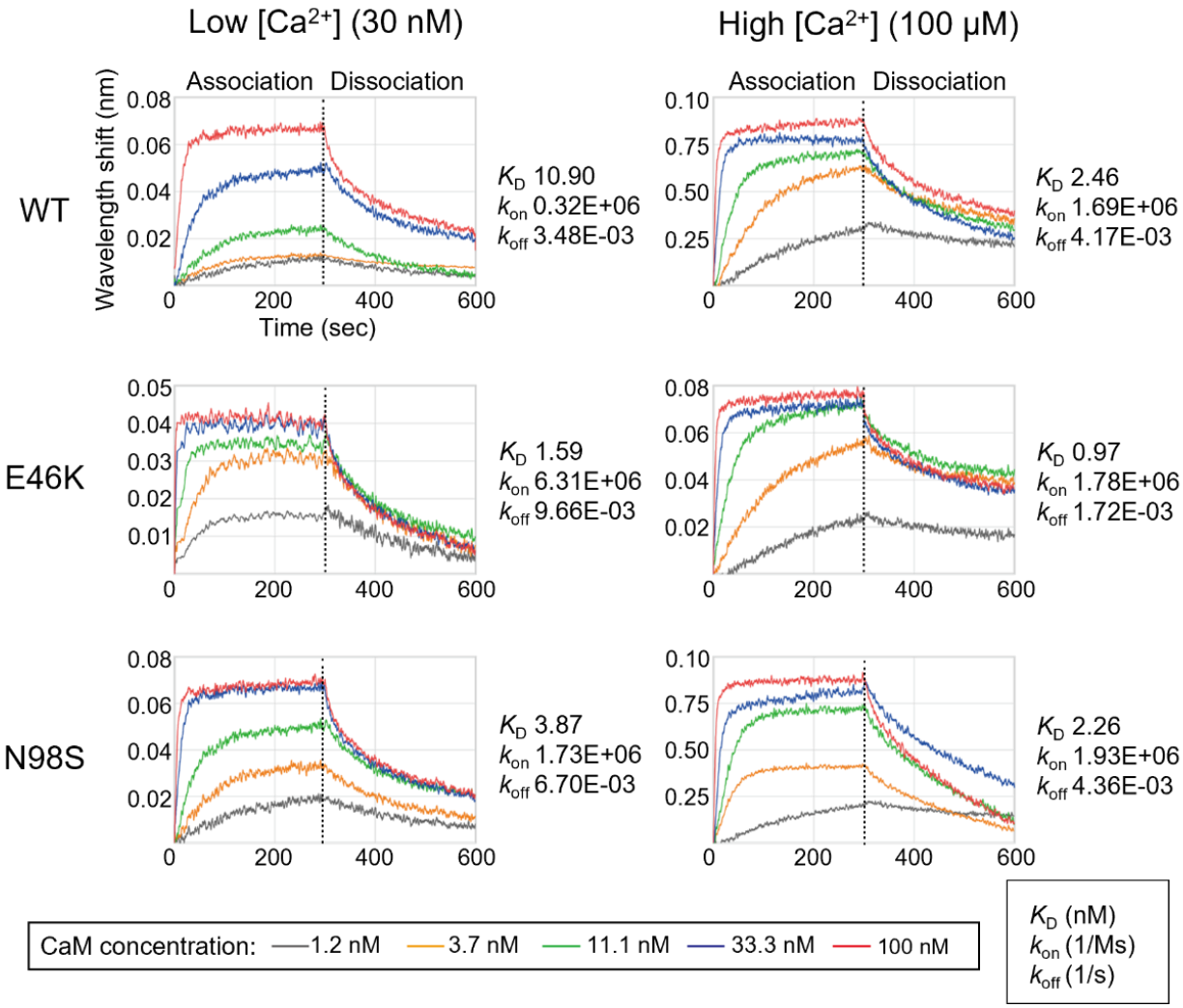

Representative traces of the real-time binding response between RyR2 and various CaMs (WT, E46K, or N98S) obtained by the BLI-based Octet RED 96 system. The traces are shown after subtracting nonspecific binding recorded under CaM-free solution. Dashed lines indicate the boundary between the association and dissociation steps. Data were processed and curve fitting was performed using a 1:1 binding model by Octet Data Analysis Software to obtain the kinetic parameters such as the association (k_{on}) and dissociation (k_{off}) rate constants, and the binding affinity constant ($K_D = k_{off}/k_{on}$).

Supplemental Figure XII

L-type Ca^{2+} current recordings in *CALM2*-E46K iPSC-CMs

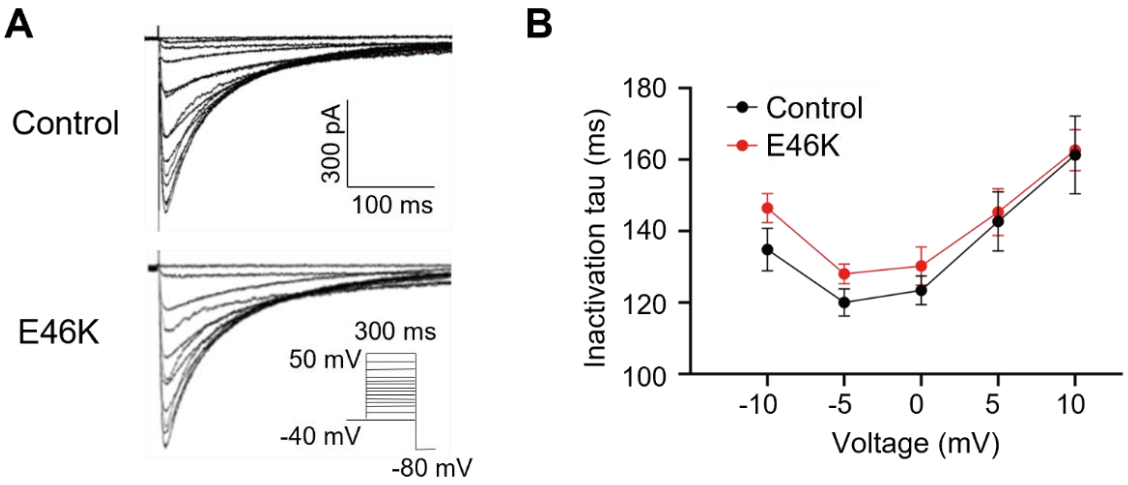

(**A**) Representative traces of the L-type Ca^{2+} current (I_{CaL}) in the control and *CALM2*-E46K iPSC-derived cardiomyocytes (iPSC-CMs). (**B**) The time constants of inactivation in the control (black) and *CALM2*-E46K (red) iPSC-CMs. Data are shown as means ± SEM from the control ($n = 7$) and E46K ($n = 8$) which were analyzed by two-tailed unpaired *t*-test. There is no significant difference between the two cell lines.

Supplemental Figure XIII

Three-dimensional mapping of CPVT-related *CALM* variants on CaM-RyR2 complex structures

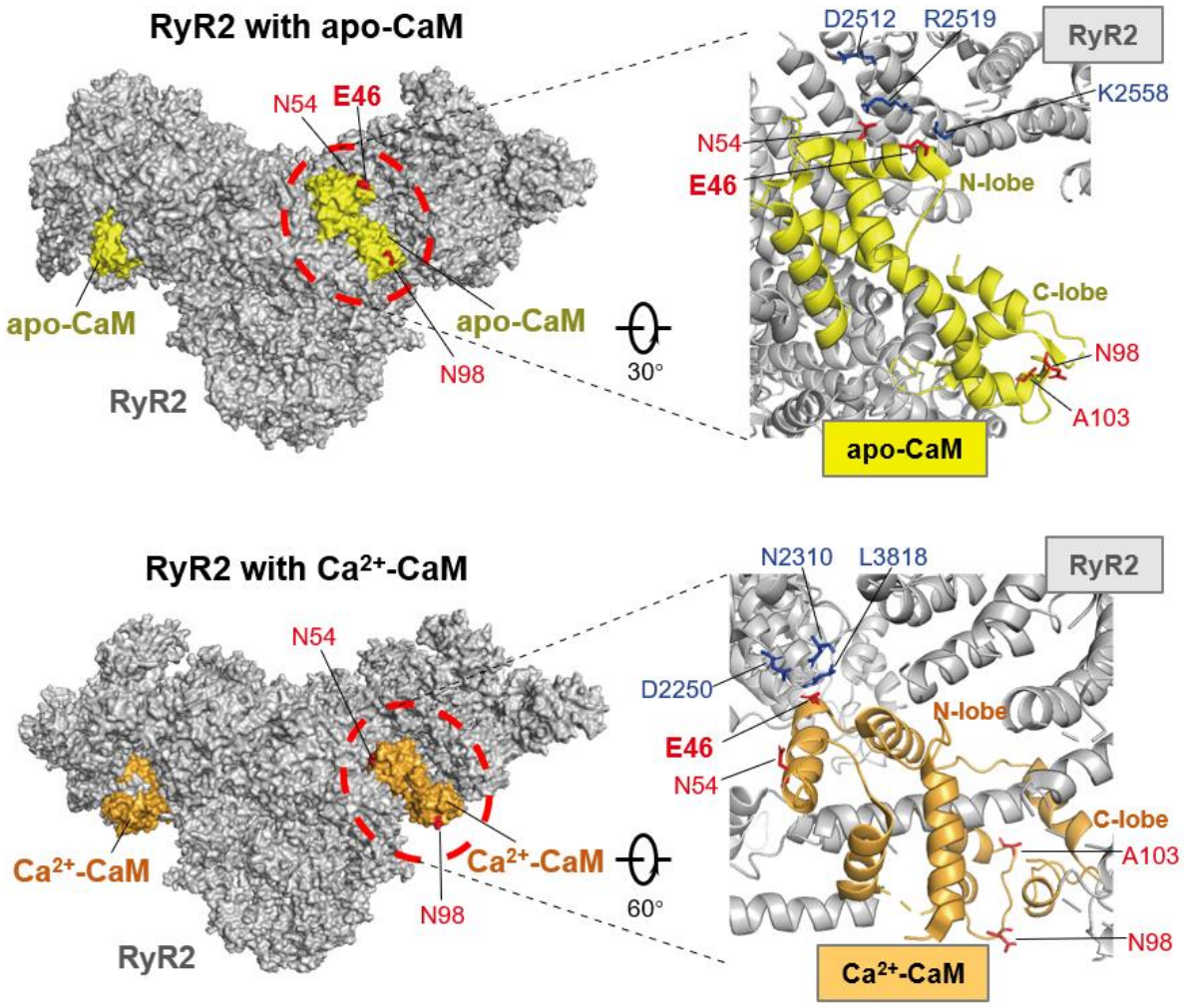

CPVT-associated *CALM* variants (E46K, N54I, N98S, and A103V) were mapped onto two CaM-RyR2 complex structures, apo-CaM-RyR2 (PDB code: 6JI8) and Ca^{2+}-CaM-RyR2 (PDB code: 6JIY), using PyMOL (version 2.1.1). The proteins are highlighted as RyR2 in gray, apo-CaM in yellow (upper), and Ca^{2+}-CaM in orange (lower). The CaM-RyR2 interaction areas are shown enlarged (right). The amino acids associated with the *CALM* variants are shown in red text and the neighboring amino acids in RyR2 are shown in blue text.